LIDAR AIDED CAMERA CALIBRATION IN HYBRID IMAGING AND MAPPING SYSTEMS

By

ABHINAV SINGHANIA

A THESIS PRESENTED TO THE GRADUATE SCHOOL
OF THE UNIVERSITY OF FLORIDA IN PARTIAL FULFILLMENT
OF THE REQUIREMENTS FOR THE DEGREE OF
MASTER OF SCIENCE

UNIVERSITY OF FLORIDA

2007

Dedicated to my mother, father and brother

ACKNOWLEDGMENTS

I would like to thank my professors: William Carter, Ramesh Shrestha and Clint Slatton for their support and encouragement throughout my study. Dr Ramesh Shrestha provided the much needed guidance and support towards the completion of this work. The direction, insight and critique provided by Dr William Carter were quintessential and appreciated.

I would also like to express my gratitude towards Sidney Schofield and Scott Miller for flying and collecting the data required for the study. Finally I would also like to thank Donald Moe from USGS for his inputs.

TABLE OF CONTENTS

LIST OF TABLES

Table page

LIST OF FIGURES

Figure page

Abstract of Thesis Presented to the Graduate School
of the University of Florida in Partial Fulfillment of the
Requirements for the Degree of Master of Science

LIDAR AIDED CAMERA CALIBRATION IN HYBRID IMAGING AND MAPPPING SYSTEMS

By

Abhinav Singhania

December 2007

Chair: Ramesh Shrestha
Major: Civil Engineering

Advancement in the fields of position and navigation systems has made possible the tracking of a moving platform with an accuracy of a few centimeters. This in turn has led to the development of the concept of direct georeferencing with the aid of Inertial Measurement Unit (IMU) and Differential Global Positioning System (DGPS). The aerial mapping systems have expanded their scope from aerial photography to include laser scanning systems, popularly known as LIDAR, which use laser pulses to map the earth surface resulting in high resolution surface models.

The present century has seen the successful introduction and use of hybrid imaging and mapping systems which typically consist of a laser scanner and a digital camera mounted together on a platform. The strength of such systems lies in the use of two sensors that complement each other well. The laser scanning system provides high resolution and accurate three-dimensional positions, whereas the digital camera provides textural and spectral information.

The successful co-registration of such systems depends on the accurate calibration of the mapping systems. Camera calibration is one such important component of this mapping process. Calibration includes the relative position and orientation of the camera with respect to the other

sensors in the mapping system, as well as the internal geometry/orientation of the camera. Previously, aerial mapping was limited to the use of metric cameras, but in recent years some users have elected to work with less expensive, small format " " cameras, for which the internal orientation of the camera assumes a higher significance. Various procedures have been introduced and studies carried out to study the use of nonmetric cameras in mapping. One conclusion reached by virtually all investigations is that careful calibration of the camera at frequent intervals is essential.

This thesis reports on a study carried out at the Geosensing Systems Engineering Research Center at the University of Florida, which explores the use of LIDAR data in the calibration of digital cameras. Two different cases are studied, one using a terrestrial mapping system and another using an airborne mapping system. The calibration is performed with the aid of LIDAR data and the results are examined by evaluating the accuracy in positions of the control points obtained from georeferenced images.

CHAPTER 1
INTRODUCTION

Background

Aerial Mapping

Aerial mapping has evolved into a relatively efficient and accurate method for producing topographic maps. Within the past decade, film based cameras have phased out and replaced by the widespread use of digital imaging sensors. Moreover with the use of position (Differential Global Positioning System, DGPS) and navigation sensors (Inertial Measurement Unit, IMU) in recent years, combined with an array of digital imaging sensors available such as digital cameras, hyperspectral/multispectral cameras, LIDAR (Light Detection and Ranging) imaging sensors and SAR (Synthetic Aperture Radar), a marked transformation has taken place in the approach to the problem of image georeferencing.

The traditional procedure for aerial mapping involved collecting images with at least 60% forward overlap and 30% side overlap, which were used to form contiguous stereo models covering the area of interest (Wolf and Dewitt, 2000). Traditional surveying methods were used to establish Ground Control Points (GCPs). The GCPs and their corresponding image pixel coordinates were used to perform 'Aerotriangulation' using the principle of space resection to estimate the position and the orientation of the aerial camera sensor. A mathematical model, derived from collinearity equations using the orientation and position parameters, was used to georeference the image. This procedure is known as space intersection. The position and orientation parameters together constitute the exterior orientation parameters (EOP) of the imaging sensor (Wolf and Dewitt, 2000).

Advances in the field of GPS and navigation sensors and their use in aerial mapping have realized the concept of Direct Image Georeferencing (Dorota A, 2001; Cramer, 2001; Bäumker

et al. 2002). These sensors provide direct measurements for EOP. Direct georeferencing has proven advantageous because it eliminates the need for using a large number of ground control points (GCP), greatly reducing the costs associated with establishing them. Moreover it makes possible the aerial mapping of otherwise inaccessible remote areas (Cramer, 2001). GPS and IMUs have also made possible the use of aerial imaging sensors such as LIDAR and SAR. Moreover different imaging sensors can be used simultaneously on the same aircraft, complementing each other. For example LIDAR provides accurate three dimensional (3D) position data in the form of X,Y, Z point clouds or a Digital Elevation Model (DEM), Charge Coupled Devices (CCD) sensor based multi-spectral cameras can provide spectral data over a wide range of wavelengths..

Today, a typical aerial mapping system may consist of a digital multispectral camera, a laser scanning system, a high accuracy GPS receiver, and an IMU. Each of the instruments must be calibrated and their relative positions must be accurately determined. The various geometrical aspects that must be considered for calibration include:

- Lever arm offsets between the camera sensor and the GPS antennae reference point
- Angular misalignment between the coordinate systems of the imaging sensor and the IMU system—also known as Boresight angles

Apart from these, if a camera is used the internal orientation parameters also need to be calibrated (principal point coordinates and focal length; Cramer, 2001).

The lever arm offsets are generally determined using total station or other ground surveying instruments. In the case of an IMU system integrated into the imaging sensor, the angular misalignment calibration may be done in the lab once and then checked at regular intervals. However, if the IMU sensors are mounted separately from the imaging sensor, the calibration needs to be checked each time either of the sensors is removed from the aircraft.

The internal orientation parameters of a non-metric camera are also generally determined in a laboratory using a calibration test field. However, these cameras have an unstable interior geometry. Potential error sources include the movement of the CCD sensor and the lens mounts with respect to camera body (Fraser, 1997; Ruzgienė, 2005). These movements though minute in nature, are significant enough to affect the interior orientation parameters. Also, these parameters are determined in laboratories under constant and homogenous temperature and pressure conditions. In actual flight conditions, these conditions vary and can cause non-negligible lens deformations and distortions (Karsten et al, 2005). Hence, the accuracy and stability of the interior orientation parameters is always questionable.

Ground Based Terrestrial Mapping

In the past, ground based data collection using close range photogrammetric techniques was largely limited to such fields as architecture, heritage data collection, and geology. Data collection was done using cameras. The information obtained was mainly 2D. Later 3D information was extracted using multiple images and stereoscopic principles. The start of the present century saw the use of ground based laser scanners becoming popular. Also known as terrestrial laser scanners, they provide high density point clouds (position information) together with monochrome intensity data, reaching high accuracy levels. Their applications have expanded to the fields of civil engineering, forestry, beach erosion studies and archeology, to name a few (Drake, 2002; Fernandez, 2007). Similar to the airborne mapping systems, recent years have seen a shift towards hybrid terrestrial imaging systems that simultaneously acquire data using a digital camera as well as a laser scanner (Ulrich et al, 2003; Jansa et al, 2004). The laser data not only enhances the data acquired but can also assist in the calibration. With the millimeter level positional accuracy of terrestrial laser systems (Optech product specifications), it provides a 3D calibration field for external as well as the internal calibration of the camera.

The basic photogrammetric principles for the data fusion in these hybrid systems remain the same as for the airborne systems. Here too, the importance of the calibration of the relative geometry of the two sensors cannot be overemphasized. It involves the determination of the parameters for the registration of the image to the coordinate system of the laser scanner. These parameters are:

- Relative linear position of the origins of the coordinate systems of the laser scanner and the CCD sensor
- Angular misalignment between the two coordinate systems.
- Interior orientation parameters for the camera

Objective

The integration of LIDAR and digital camera provides beneficial prospects not only for the purpose of data fusion but also camera calibration. The DEM (Digital Elevation Model) as well as the intensity image produced from airborne LIDAR data provides useful information for calibration. The former can be used to obtain the actual ground elevation to establish an accurate scale and the latter can provide ground control points for calibration. In the case of terrestrial LIDAR systems, where the point density reaches much higher than the airborne systems (about 10^4 per m^2), the points themselves can be used to provide control for calibration.

The GEM (Geosensing Engineering and Mapping) research center at the University of Florida owns an airborne laser mapping system, ALTM 1233 and a terrestrial laser mapping system, ILRIS3D, both manufactured by Optech Incorporated, a Canadian company. The research center also acquired a 4-band multi-spectral non-metric camera, Redlake MS4100, for combined airborne laser and digital photography mapping. Although the ILRIS3D has a built-in digital camera, the full advantage of its hybrid capability is not realized because of low quality of the images (low resolution and limited colour balance). So, UF recently purchased a non-metric

10.2 megapixel digital SLR camera: Nikon D80, equipped with a 20mm focal length lens, to use with the ILRIS3D.

This thesis explains a study performed to demonstrate the use of LIDAR data as an aid for performing on-the-job calibration of non-metric digital cameras used for aerial as well as terrestrial mapping in hybrid imaging systems. Various issues concerned with this application, such as parameters affecting the strength of calibration, the effect of LIDAR accuracy on the calibration, the accuracy of the georeferenced imagery, and practical usefulness of the procedure, are also discussed.

Chapter 2 introduces the concepts behind image georeferencing. The camera models and calibration fundamentals are explained in Chapter 3. In Chapters 4 and 5, the study that was carried out is presented. Finally, Chapter 6 summarizes and concludes the thesis

CHAPTER 2
IMAGE GEOREFERENCING

Image georeferencing implies the transformation of image coordinates with respect to the image coordinate system to the 3D coordinates in the mapping reference frame or the geodetic reference frame. This is carried out by using extended collinear equations given below (Wolf & Dewitt, 2002; Pinto et al, 2002):

$$X_m = X_c + \lambda (r_i^m (X_i))$$

Where, X_i = 2D image coordinates in imaging frame

X_m = corresponding 3D coordinates in the mapping frame

X_c = 3D coordinates of the sensor in the mapping frame, perspective center of the camera

λ = scale factor

r_i^m = rotation matrix for conversion from image frame to mapping frame

As the equation suggests, the position and orientation of the camera at the time of exposure are the two parameters required for georeferencing, which need to be determined. These parameters can be obtained in two ways:

- Indirect Georeferencing using control points: Also known as the space resection principle, it involves using control points whose coordinates on the image as well as in the mapping frame are known. A minimum of 4 points are required to obtain a solution for the 7 parameters i.e. the X,Y,Z position of the camera, the three rotation angles for transformation and the scale factor. If 5 or more control points are used, a least squares solution can be obtained. This procedure is used for georeferencing the terrestrial mapping system
- Direct Georeferencing /Direct Sensor Orientation: This involves the use of position (DGPS) and inertial sensors (IMU) to obtain the two set of parameters. The collinear equation needs to be modified to include the information given by the position and navigation sensors. This is used in the case of the airborne mapping system

Indirect Georefencing as Applied to Terrestrial Mapping System

The reference frames involved are as follows (figure 2.1):

- Object mapping frame, representing the reference frame in which the point cloud is represented.
- Intermediate frame
- Camera frame: frame misaligned with the intermediate frame by misalignment angles θ, φ, γ about X, Y and Z axes respectively. .

The coordinate transformations involved between these frames are given by;

1. Object mapping frame to Intermediate frame: C_m^t: $\begin{bmatrix} 0 & 0 & -1 \\ -1 & 0 & 0 \\ 0 & 1 & 0 \end{bmatrix}$

2. Intermediate frame to Camera frame: C_t^c, (Rogers, 2003):

$$\begin{bmatrix} \cos\gamma\cos\varphi & \cos\gamma\sin\varphi\sin\theta+\sin\gamma\cos\theta & \sin\gamma\sin\theta-\cos\theta\sin\varphi\cos\gamma \\ -\sin\gamma\cos\varphi & \cos\theta\cos\gamma-\sin\theta\sin\varphi\sin\gamma & \sin\gamma\sin\varphi\cos\theta+\cos\gamma\sin\theta \\ \sin\varphi & -\cos\varphi\sin\theta & \cos\varphi\cos\theta \end{bmatrix}$$

where θ, φ, γ are rotations about X, Y and Z axes respectively in the same order.

Therefore the rotation matrix for transforming from the Object mapping frame to Camera frame is:

$$C_m^c = C_t^c \, \mathrm{x} \, C_m^t$$

Once the orientation parameters are known, the extended collinear equation is then used to georeference the image:

$$\begin{bmatrix} Xi - X_L \\ Yi - Y_L \\ Zi - Z_L \end{bmatrix} = \lambda(C_c^m) \begin{bmatrix} xi \\ yi \\ zi \end{bmatrix}$$

where

xi, yi, zi : Image pixel coordinates in the camera frame

X_L, Y_L, Z_L : Coordinates of the camera in the mapping frame

X_i, Y_i, Z_i : Coordinates of the image pixel in mapping frame

λ= scale factor

$C_c^m = C_m^{c'}$, Rotation matrix from camera to object mapping frame

Direct Georeferencing as Applied to Airborne Mapping System

DGPS gives the position of the airplane in the mapping frame. The IMU however gives the orientation in terms of roll, yaw and pitch in the inertial reference frame (figure 2.2). They need to be transformed from the inertial frame to the mapping frame. Thus the collinearity equations are modified to include the coordinate transformations related to the navigation information. The coordinate frames involved (figure 2.3) in the transformations are (Bäumker et al, 2001):

1. Mapping reference frame representing the geodetic mapping frame
2. Navigation frame, represents the north east down (NED) frame. The orientation of the airplane in terms of yaw(θy), pitch (θp) and roll (θr) is given with respect to this frame.
3. Body frame, represents the actual orientation given by IMU. Ideally, IMU would be strapped to the sensor itself so as to have the orientation of the sensor itself which is generally the case in single imaging sensor systems. The accelerations acc_x, acc_y, acc_z, are measured by the IMU in this frame.
4. Imaging Sensor/Camera frame, represents the orientation of the camera and is misaligned to the body frame by the boresight angles represented by misalignment in pitch(θ_{pm}), roll (θ_{rm}) and, yaw (θ_{ym}).
5. Image frame in which the pixel coordinates are given.

The coordinate transformations and their order involved to go from a mapping frame to image frame are as shown in figure 3.

Rotation transformation matrix from mapping frame to image frame is given by (Rogers, 2003)

$$C_m^i = C_c^i \times C_b^c \times C_n^b \times C_m^n$$

Where

$$C_m^n = \begin{bmatrix} 0 & 1 & 0 \\ 1 & 0 & 0 \\ 0 & 0 & -1 \end{bmatrix}$$

$$C_n^b = C_b^{n'} = \begin{bmatrix} \cos\theta y \cos\theta p & \cos\theta y \sin\theta p \sin\theta r - \sin\theta y \cos\theta r & \cos\theta y \sin\theta p \cos\theta r + \sin\theta y \sin\theta r \\ \sin\theta y \cos\theta p & \sin\theta y \sin\theta p \sin\theta r + \cos\theta y \cos\theta r & \sin\theta y \sin\theta p \cos\theta r - \cos\theta y \sin\theta r \\ -\sin\theta p & \cos\theta p \sin\theta r & \cos\theta p \cos\theta r \end{bmatrix}'$$

$$C_b^c = C_c^{b'} = \begin{bmatrix} \cos\theta ym \cos\theta pm & \cos\theta ym \sin\theta pm \sin\theta rm - \sin\theta ym \cos\theta rm & \cos\theta ym \sin\theta pm \cos\theta rm + \sin\theta ym \sin\theta rm \\ \sin\theta ym \cos\theta pm & \sin\theta ym \sin\theta pm \sin\theta rm + \cos\theta ym \cos\theta rm & \sin\theta ym \sin\theta pm \cos\theta rm - \cos\theta ym \sin\theta rm \\ -\sin\theta pm & \cos\theta pm \sin\theta rm & \cos\theta pm \cos\theta rm \end{bmatrix}'$$

$$C_c^i = C_m^{n'} = \begin{bmatrix} 0 & 1 & 0 \\ 1 & 0 & 0 \\ 0 & 0 & -1 \end{bmatrix}'$$

For ease of writing elements of C_m^i will be represented as

$$C_m^i = \begin{bmatrix} r_{11} & r_{12} & r_{13} \\ r_{21} & r_{22} & r_{23} \\ r_{31} & r_{32} & r_{33} \end{bmatrix}$$

Rotation from image to mapping frame is given by

$$C_i^m = C_m^{i'}$$

Once all the EOP and the boresight angles are known the following equation may be used to georeference the images:

$$\begin{bmatrix} Xi - Xp \\ Yi - Yp \\ Zi - Zp \end{bmatrix} = \lambda (C_i^m) \begin{bmatrix} xi \\ yi \\ zi \end{bmatrix}$$

Where

Xi, Yi and Zi = mapping frame coordinates to be determined

Xp, Yp, Zp = imaging sensor position coordinates in the mapping frame

λ = scale factor

xi, yi = image pixel coordinates

zi = -f(focal length)

C_i^m = rotation matrix for coordinate transform from image frame to mapping frame

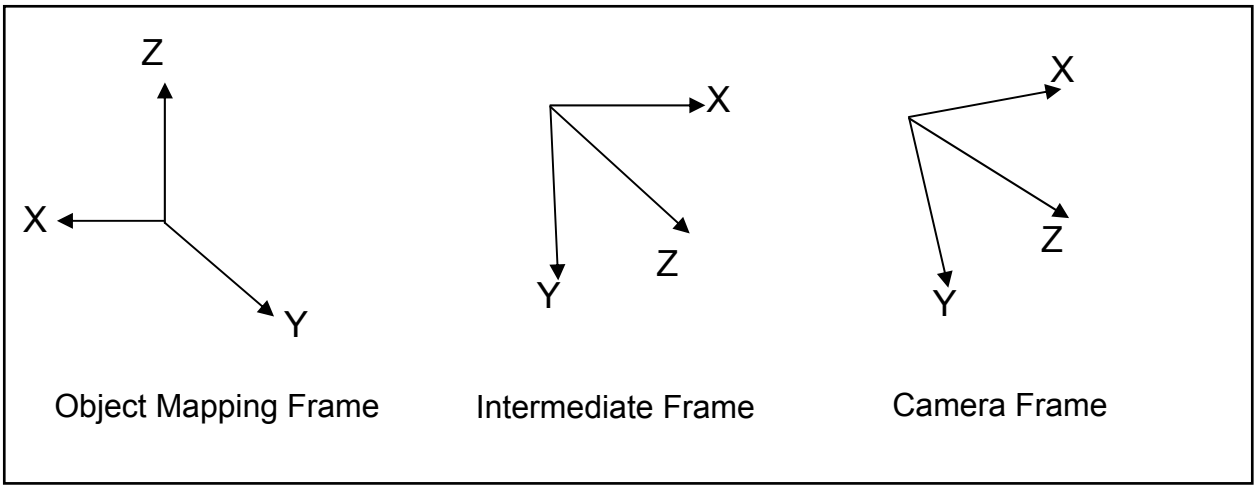

Figure 2.1 Coordinate frames for terrestrial system

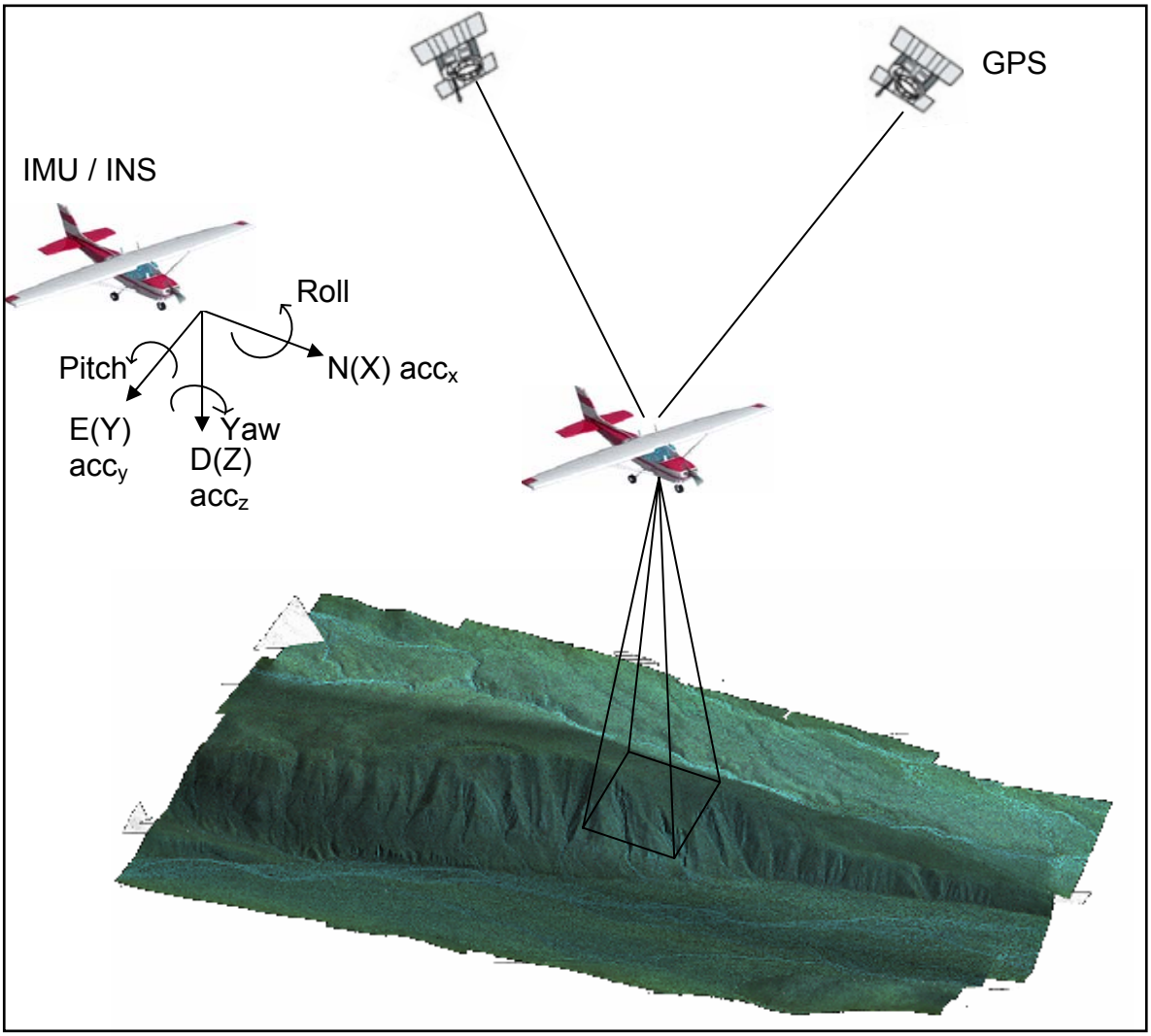

Figure 2.2 Direct Georeferencing

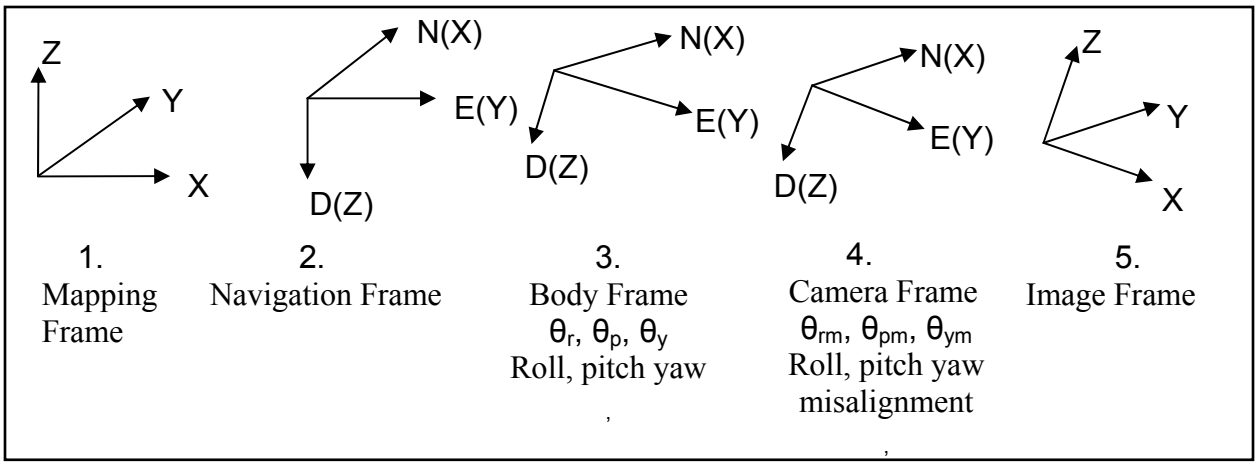

Figure 2.3 Coordinate Systems in Direct Referencing

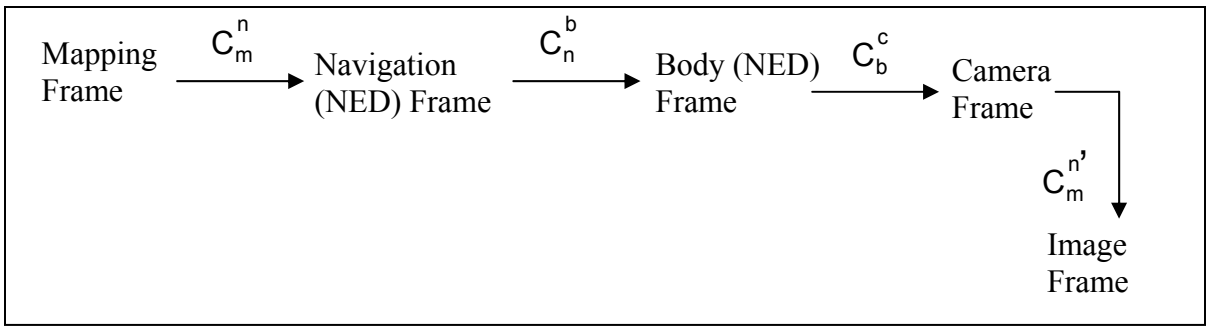

Figure 2.4: Coordinate transformation in Direct Sensor Orientation

CHAPTER 3
CAMERA CALIBRATION

Introduction

Calibration is the determination of the orientation of the camera, external as well as internal, so that the image coordinates can be transformed to real world mapping coordinates to derive object space information (Gruen, 2001).

The issue of calibration was discussed by early photogrammetrists as a problem of determining camera orientation. In 1859 Aimè Laussedat in France used a theodolite to orient a camera to take images for mapping the streets of Paris. The later half of 19th century and early 20th century saw mathematicians laying down the foundations of photogrammetry which still serve as the basic principles for solving the calibration problem. In 1899 Sebastian Finsterwalder described the principles of modern double-image photogrammetry and the methodology of relative and absolute orientation. Otto von Gruber in 1924 derived the projective equations and their differentials, which are still fundamental to analytical photogrammetry.

Recent years have seen the subject of camera calibration, being tackled as a computer vision problem. This can be attributed to the increase in complexity of the problem. It has extended from just the determination of orientation of the camera to ascertaining the parameters of its internal geometry and the errors associated with digital sensors. Understanding the camera model and calibrating it has become a complex task.

Over the years various calibration procedures have evolved with the involvement of the computer vision community. However, the bundle adjustment (Brown, 1971) technique remains superior as far as photogrammetry is concerned. This point has been well discussed by Remondino and Fraser (2006). They compare the self calibration bundle adjustment procedure using corrections for distortion (Fraser, 1997; Gruen et al, 2001) to other techniques such as

DLT/linear techniques (Abdel-Aziz et al, 1971) and linear/nonlinear combination techniques (Tsai, 1987; Heikkilä & Silven, 1997). Better results were obtained by the bundle adjustment technique as compared to the other methods; the basis of comparison being the root mean square error (RMSE) values of calculated object point coordinates against their true observed values. Thus the motivation behind the use of bundle adjustment within this research as the chosen technique to carry out camera calibration.

Camera Model

Before undertaking the task of calibration, it is important to understand the camera model so as to identify the parameters that need to be determined. The camera model can be either projective or perspective collineation. The bundle adjustment uses the perspective model. However, both models are discussed briefly below (for more information, refer Appendix A).

Projective Collineation Camera Model

A general projective model maps an object point **X** to an image point **x** according to **x** = P **X**. P is a 3x4 matrix which can be decomposed as P = K I M (Mohr et al, 2001; Remondino & Borlin, 2004)

where,

K = $\begin{bmatrix} f_x & s & x_0 \\ 0 & f_y & y_0 \\ 0 & 0 & 1 \end{bmatrix}$ is an upper triangular matrix with the interior parameters of the camera

fx and *fy* are the focal length along x and y axis

s the skew factor

(*x0*, *y0*) the principal point position;

$$I = \begin{bmatrix} 1 & 0 & 0 & 0 \\ 0 & 1 & 0 & 0 \\ 0 & 0 & 1 & 0 \end{bmatrix}$$

M = [R|T], gives the position and orientation of camera

R is a rotation matrix

T is translation vector.

If the camera is fixed and undergoes only rotations (co-centric images or negligible eccentricity), we can eliminate the vector t and express the mapping of **X** onto **x** as

x = K I R **X** as P = K I R.

The coordinates (x, X) are defined as homogeneous coordinates, explained in the Appendix A (Mohr et al, 2001).

The most important benefit of projective model is the linear relationship in the equations. Moreover, it can also handle variable focus and zoom optics of the camera. However it has drawbacks such as less stability in equations, requirement of large number of parameters and most importantly complexities involved in dealing with non-linear lens distortions (Frasier 2001; Remondino & Fraser, 2006). Also it does not define the coordinates in a 3D metric space (Fraser, 2001). All these render it unusable for high accuracy photogrammetric mapping. Still there are other areas which give more priority to other criterion such as short processing time and do not require object points position in 3D metric space. It is widely used in applications such as autonomous vehicle navigation, robotic vision, medical imaging etc.

Perspective Collineation Camera Model

The perspective collineation model is the most widely used camera model for photogrammetric mapping purposes. It is also derived from the basic collinear equations. Collinearity is a condition where in the exposure station, the object point and its image, all lie on

the same straight line. This condition can be exploited to arrive at the camera model as described in Appendix A (Wolf and Dewitt, 2002). The model itself is given below:

$$xi - x_0 = -f\left[\frac{r_{11}(X_L - Xo) + r_{12}(Y_L - Yo) + r_{13}(Z_L - Zo)}{r_{31}(X_L - Xo) + r_{32}(Y_L - Yo) + r_{33}(Z_L - Zo)}\right]$$

$$yi - y_0 = -f\left[\frac{r_{21}(X_L - Xo) + r_{22}(Y_L - Yo) + r_{23}(Z_L - Zo)}{r_{31}(X_L - Xo) + r_{32}(Y_L - Yo) + r_{33}(Z_L - Zo)}\right]$$

where,

f : focal length of the camera.

X_L, Y_L and Z_L: perspective center coordinates in object mapping frame

Xo, Yo and Zo: object coordinates in the mapping frame;

x_i, y_i, z_i: image coordinates in image frame

x_0 and y_0: displacement in the principal point position with respect to the center of the image plane

Calibration Parameters

The calibration parameters consist of the exterior orientation parameters and interior orientation parameters.

Exterior Orientation Parameters

The exterior orientation parameters are basically the 3 translations along the coordinate axes and the 3 rotational misalignments about the coordinate axes between the imaging sensor coordinate system and the object mapping coordinate system. However the exact parameters which are determined differ in the case of airborne and terrestrial mapping system.

Incase of an airborne mapping system the position is provided by the GPS sensor. The translational elements of the orientation are therefore given in terms of displacement of the camera along the X, Y and Z axis from the phase center of the GPS antenna. The orientation is

provided by an IMU in terms of roll, pitch and yaw in an inertial frame of reference. However there always exist an angular misalignment between the orientations of the imaging sensor (digital camera) reference frame and the IMU. These are calculated as misalignments in roll (θ_{rm}), pitch (θ_{pm}) and yaw (θ_{ym}) and constitute the exterior orientation parameters for airborne mapping systems. Mathematically they form the transformation matrix of body frame to camera frame (C_b^c) that was presented in chapter 2. They are further introduced into the camera model embedded in the elements of rotation matrix C_m^i (mapping to image frame).

In a terrestrial mapping system the point clouds are collected in a scanner coordinate system defined by the orientation of the laser scanner and an origin which is a manufactured specified point of reference on the instrument. The translational orientation parameters are given by the position of the camera as defined in this coordinate system. The angular orientation parameters are given as misalignments (θ along X, φ along Y and γ along Z axes) between the camera and the laser scanner as represented in the same scanner coordinate system.

Interior Orientation Parameters

They define the relationship between the perspective center of the imaging sensor and the image coordinates. There are basically three parameters of interior orientation:

- The principle distance or the focal length, f: It is the perpendicular distance of the perspective center to the projection plane
- Principle point coordinates: They are the x and y coordinates of the point where the perpendicular from the perspective center intersects the projection plane. The principle point should ideally be coincident with the origin of the image coordinate system defined by the center of the image (the central row and column for a CCD image), which is not the case in most of the cameras.

The interior orientation parameters can also be specified as the coordinates (x, y, f) of the perspective center in the image coordinate system.

Additional Parameters

These parameters account for the distortion effects in the non-metric camera and are included as an additional displacement of the image pixel Δx and Δy along x and y axis in the image coordinate system. The two distortion effects taken into consideration are (Fraser, 2001):

- Radial lens distortion: It is represented as an odd numbered polynomial series (as a result of Seidel aberrations) given as

  $\Delta r = K_1 r^3 + K_2 r^5 + K_3 r^7 \ldots..$

  where K_i are the distortion coefficients and r is the radial distance from the principal point ($r^2 = x^2 + y^2$). The correction to the image coordinates is given as

  $\Delta x_r = x\Delta r/r$ and $\Delta y_r = y\Delta r/r$.

  Generally for medium accuracy applications K_1 is sufficient and for high accuracy applications K_2 and K_3 may be used but are not necessarily significant for every case.

- Decentering distortion: This is a result of the lack of centering of the lens element along the optical axis. It causes both radial and tangential image displacements. It is modeled by correction equations given by Brown:

  $\Delta x_r = P_1 (r^2 + 2x^2) + 2P_2 xy$
  $\Delta y_r = P_2 (r^2 + 2y^2) + 2P_1 xy$

  where P_1 and P_2 are distortion coefficients

K_1, K_2, K_3, P_1 and P_2 form the additional parameters which need to be calculated. Other form of distortion effects like that due to image plane unflatness and in plane image distortions are negligible in magnitude and have no metric effect (Fraser, 1997).

Calibration Procedure

The collinearity equations derived above for the perspective camera model are given as (Gruen & Beyer, 2001):

$$xi - x_0 - \Delta x = -f\left[\frac{r_{11}(X_L - Xo) + r_{12}(Y_L - Yo) + r_{13}(Z_L - Zo)}{r_{31}(X_L - Xo) + r_{32}(Y_L - Yo) + r_{33}(Z_L - Zo)}\right]$$

$$yi - y_0 - \Delta y = -f\left[\frac{r_{21}(X_L - Xo) + r_{22}(Y_L - Yo) + r_{23}(Z_L - Zo)}{r_{31}(X_L - Xo) + r_{32}(Y_L - Yo) + r_{33}(Z_L - Zo)}\right]$$

Rearranging

$$xi = -f\left[\frac{r_{11}(X_L - Xo) + r_{12}(Y_L - Yo) + r_{13}(Z_L - Zo)}{r_{31}(X_L - Xo) + r_{32}(Y_L - Yo) + r_{33}(Z_L - Zo)}\right] + x_0 + \Delta x \quad \text{.....(3.1)}$$

$$yi = -f\left[\frac{r_{21}(X_L - Xo) + r_{22}(Y_L - Yo) + r_{23}(Z_L - Zo)}{r_{31}(X_L - Xo) + r_{32}(Y_L - Yo) + r_{33}(Z_L - Zo)}\right] + y_0 + \Delta y \quad \text{.....(3.2)}$$

These act as the observation equations for the least square analysis for calibration. They result in the following cases depending on which parameters are treated either as unknowns or known a priori (Gruen & Beyer, 2001):

- General Bundle Method: All parameters on the right hand side are unknown (interior orientation, exterior orientation, object point coordinates)
- Bundle method for metric camera: The interior orientations (x_0, y_o and f) are known and all others need to be determined
- Spatial resection: object point coordinates are known, interior and exterior orientation parameters need to be determined.
- Spatial intersection: The interior and exterior orientations are known and the object point coordinates need to be determined, the case for achieving georeferencing of images.

The cases for the airborne mapping system and the terrestrial mapping systems differ. For the airborne system, the position of the imaging sensor (X_L, Y_L, Z_L) is known and tie points between the images are used together with a minimal number of control points (points with known object point position). The analysis therefore is a combination of a partial general bundle method and spatial resection also known as 'Self Calibrating Bundle Adjustment'. In the case of a terrestrial mapping system, only control points are used for solving orientation parameters. Therefore the case is that of a spatial resection, also known as 'Test Range Calibration'.

Network Geometry for Self Calibrating Bundle Adjustment

In airborne photography, the procedure for calibration, as discussed above, involves bundle adjustment of photographs. The self calibrating bundle adjustment approach does not require control points to be well distributed in three dimensions nor does it require any ground control

(Fraser, 2001), though the use of minimal ground constraint can only improve the quality of calibration. Highly convergent network geometry however is extremely significant. It influences the accuracy of the camera calibration by decoupling the interior and exterior calibration parameters. A few characteristics of the network geometry for more accurate determinability of orientation parameters are as follows (Fraser, 2001; Remondino & Fraser, 2006)

- Variations in roll angle are required to diminish the correlation between the exterior orientation elements and the principal point location(x_0, y_0) which is achieved in airborne mapping by crossing and oblique flight lines.
- Variation in roll angles is also required to decouple the projective coupling between decentering distortion (P_1 and P_2) and x_0, y_0, although it might still exist to some extent.
- The coupling between the camera position and the principle distance/focal length is broken through introduction of scale variations. This translates to acquiring imagery at different altitudes so as to have different scale factors in the transformation from image coordinate system to object mapping coordinate system.

Least Squares Analysis

For the least square bundle adjustment, the equations 3.1 and 3.2 are linearized using Taylor's equation and put in the form (Gruen and Beyer, 2001)

$$v = A_1x_1 + A_2x_2 + A_3x_3 - L$$

where

v = vector of error in image coordinates

x_1 = parameter vector containing the orientation elements

x_2 = parameter vector containing the object point coordinates for tie points

x_3 = parameter vector containing interior orientation and additional parameter

A_1 A_2 and A_3 are respective jacobians for x_1 x_2 and x_3.

L = observed image coordinate values – calculated values obtained from Taylor's expansion

The unknowns may then be estimated as:

$$\begin{bmatrix} x_1 \\ x_2 \\ x_3 \end{bmatrix} = \begin{bmatrix} A_1{}'A_1 & A_1{}'A_2 & A_1{}'A_3 \\ A_2{}'A_1 & A_2{}'A_2 & A_2{}'A_3 \\ A_3{}'A_1 & A_3{}'A_2 & A_3{}'A_3 \end{bmatrix}^{-1} \begin{bmatrix} A_1{}'L \\ A_2{}'L \\ A_3{}'L \end{bmatrix}$$

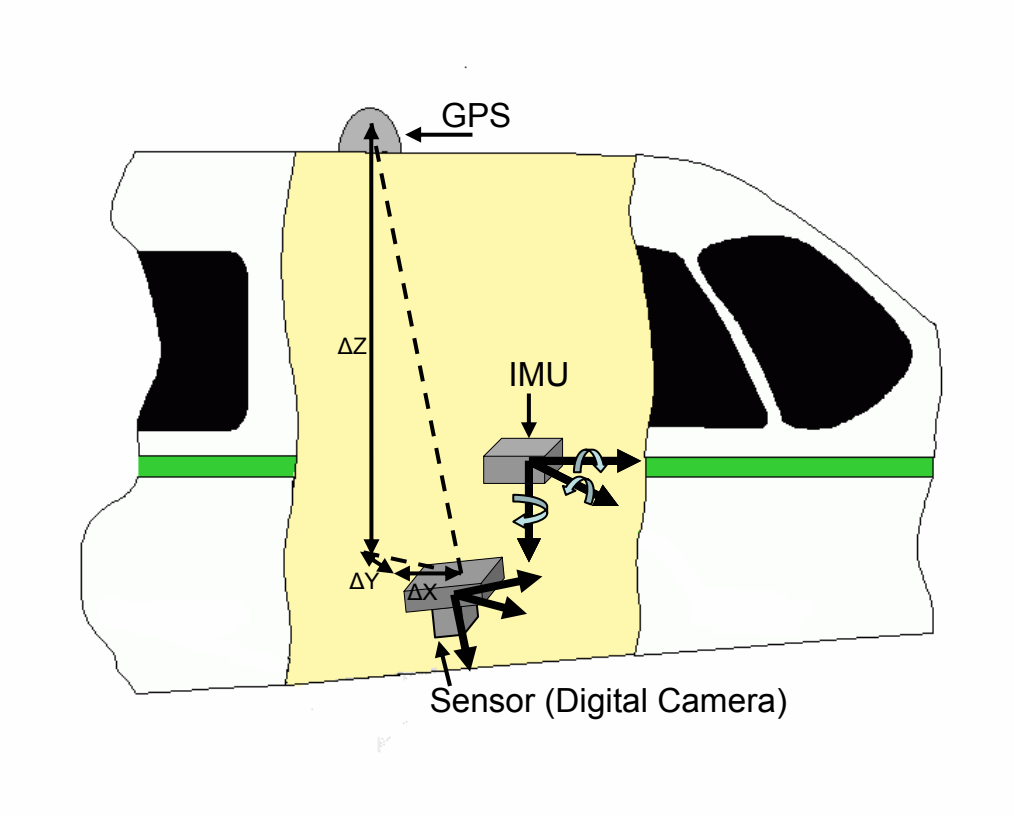

Figure 3.1 Exterior orientation elements for an airborne mapping system

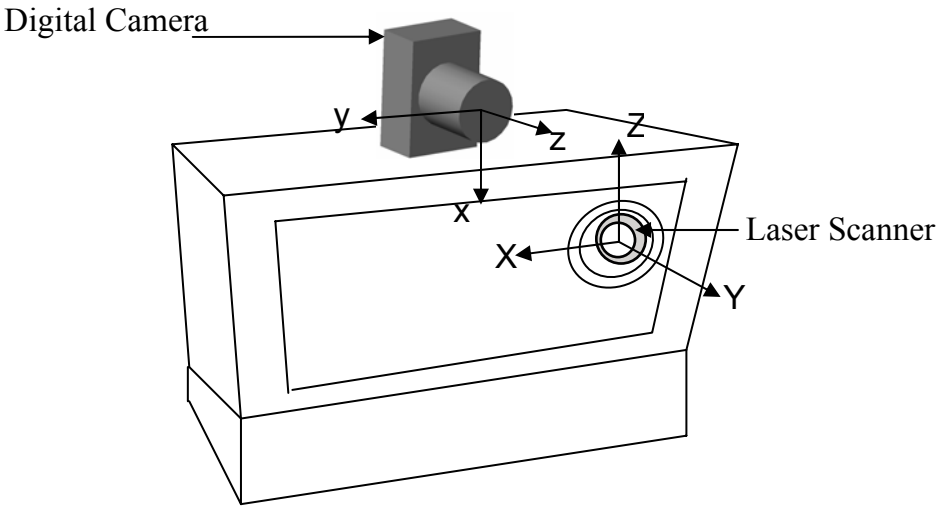

Figure 3.2 Exterior orientation parameters in a Terrestrial mapping system

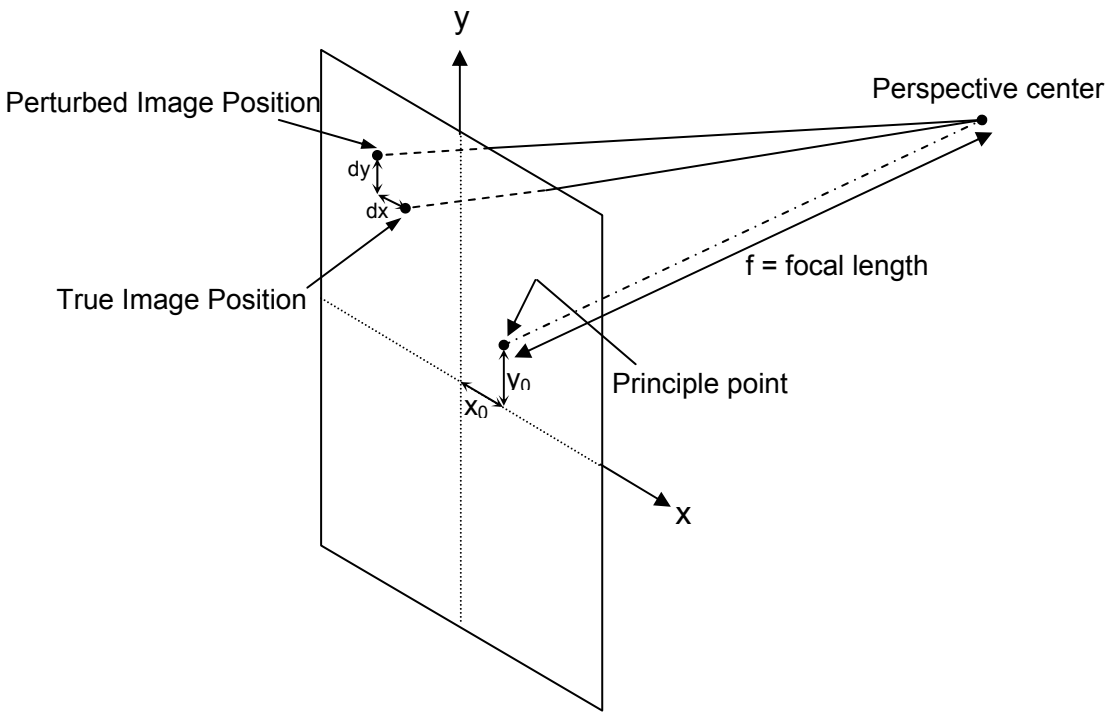

Figure 3.3 Interior orientation parameters (Fraser, 2001)

CHAPTER 4
TERRESTRIAL CAMERA CALIBRATION

Terrestrial mapping system at UF consists of the ILRIS laser imaging system and a Nikon digital SLR camera mounted on its top (Figure 4.1). The data collected by ILRIS is referenced to the mounting hole on the underside of the system (Figure 4.2). The calibration technique followed here is that of using a 3D calibration field provided by the laser data. A modified calibration as well as distortion model is used to carry out the bundle adjustment as discussed below.

Calibration Model

The calibration model used here was originally developed by Yakimovsky and Cunningham (1978) at the JPL robotics laboratory. It was later modified and improved to include distortion parameters by Grennery (2001). The model as described by Grennery (2001) is given below:

The basic model consists of 4 vectors expressed in object coordinate frame. These vectors are:

- c: the position of entrance pupil of the camera representing the positional offset from the point of reference
- a: the unit vector, perpendicular to the image sensor plane, pointing outward through the exit pupil of the camera, essentially representing the orientation of the camera
- h and v are mathematical quantities expressed as $h = h' + x_c a$ and $v = v' + y_c a$

where h' and v' are the perpendiculars to the y and x image axes respectively, in the image sensor plane (such that h', v'; and a form an orthogonal right handed system), and their magnitude equal to the change in image coordinate caused by a unit change in tangent of angle from vector a to the point viewed, p, subtended at the entrance pupil. For cameras with fixed focal length and non telephoto lens (as in the present case), it is equivalent to the distance

between the second nodal point to the sensor plane, defined in horizontal and vertical pixels. xc and yc are the image coordinates of the principle point. The terms principal points, principal planes and nodal points are described in Appendix C.

The vector 'a' would also represent the optical axis if the image sensor plane was perfectly perpendicular to it (optical axis). However, to allow for a possibility where such is not the case, a separate vector 'o' represents the optical axis.

If a vector p describes the position of a point in 3D object space, its equivalent pixel coordinates are given by

$$x = \frac{(p-c)\cdot h}{(p-c)\cdot a} \text{ and } y = \frac{(p-c)\cdot v}{(p-c)\cdot a}$$

To include effects of radial distortion, the apparent position of the point p′ is given as

$p' = p + \mu\lambda$

where, $\mu = \rho 0 + \rho 1\, \tau + \rho 2\, \tau^2$; ρ0, ρ1 and ρ2 are coefficients of distortion

$\tau = \frac{\lambda \cdot \lambda}{\varsigma^2}$; square of the tangent of the angle from optical axis to the point p

$\lambda = p - c - \varsigma o$; represents the orthogonal vector from optical axis to point p and o is the vector representing optical axis

$\varsigma = (p-c)\cdot o$; component of the vector from the principle point to

Therefore the image coordinates given for a point p′ are

$$x = \frac{(p'-c)\cdot h}{(p'-c)\cdot a} \text{ and } y = \frac{(p'-c)\cdot v}{(p'-c)\cdot a}$$

The unknowns for which the adjustment is carried out consists of vectors c, a, h, v, o and distortion coefficients ρ0, ρ1 and ρ2.

For a complete description and understanding of the model as well as the bundle adjustement algorithm, see Yakimovsky (1987) and Grennery (2001).

Calibration Data

LIDAR Data

Because LIDAR data was to be used as a 3 Dimensional calibration field, the site was chosen so as to provide points distributed in 3 dimensions, containing edges and intersections which could provide easily distinguishable control points. A section of the University of Florida football stadium met these requirements and was mapped with the laser system. Two scans were taken, first on July 17, 2007 (scan 1) and the other on August 6, 2007 (scan2). Scan1 consisted of 1,911,371 points at average point spacing of about 2.5 cm and scan 2 consisted of 1,444,665 points at the same point spacing. Each point had an intensity value to aid tie-point selection (Figure 4.3).

Initial Orientation Parameters

The initial values for the positional offsets of the camera (c_0) with respect to the point of origin of the 3D object coordinate system were approximately calculated using a measuring tape. To calculate the starting values for other unknowns, a point in the object coordinate system close to the image's centre was chosen (p_0). The camera model vectors were then calculated as follows:

$$a_0 = \text{unit}\,(p_0 - c_0)$$

$$h_0 = \frac{f}{p_{hv}}\,\text{unit}(a_0 \times u) + \frac{s_h}{2} a_0$$

$$v_0 = \frac{f}{p_{hv}}\,\text{unit}(a_0 \times h_0) + \frac{s_v}{2} a_0$$

$$o_0 = a_0$$

where

u: a vector in the object coordinate system pointing upwards i.e. [0,0,1]. f

f: focal length of the lens = 20 mm

p_{hv} : pixel size in same units as f = .006 mm

s_h and s_v: no. of rows and columns in the image respectively = 2592 x 3872

The initial value for the distortion coefficients was assigned as zero. The values of the parameters calculated as above are given below:

Control Points

Polyworks software was used to manually select control points in the point clouds and their corresponding image pixels were marked in Matlab. 20 points in scan1 (figure 4.4) and 17 points in scan 2 were distributed over the image. Their pixel coordinates and object point coordinates are as given below:

Results

The camera model parameters obtained after the bundle adjustments are given below:

Table 4.5 gives the orientation of the camera in degrees, with respect to the mapping reference frame of the laser scanner, calculated from the 'a' vector given above for each scan.

It is evident from the results that the external orientation parameter values i.e. the offsets ('c') and the angular misalignments ('a') vary and not really repeatable. This is because the camera has a single screw hole to attach it to an external mount; moreover the curvy shape of the camera on the sides makes it difficult to mount it at exactly the same place and orientation. Thus the mount is not as rigid as it should be to get repeatable mounting position and orientation.

The pixel values were extracted for the laser points and their residuals calculated for control points (Table 4.6 and Table 4.7). To ascertain the effect of distortion coefficients the pixel values for both the scans were calculated by using both sets of distortion parameters

(referred as D1 for parameters obtained from scan1 and D2 for the ones obtained form scan2). The RMS values for the residuals are given in Table 4.8

As evident by the residual as well as the RMS values, the second scan yields better results. However, the RMS values for both the scans are within the acceptable tolerances (3 pixels). Maximum RMS for scan 1 being 2.202 pixels which is approximately 6.5cms on ground (scaling at an average scan range of 105 m) and for scan 2, 1.5 pixels representing about 3.2cms on ground (scaling at an average scan range of 70m). The high (above 3 pixels) residuals in a few cases for scan 1 could probably be attributed to following reasons:

1. Ranging and position accuracy is a function of range and could be a factor of error for e.g. in case of point 18 (range = 126m)
2. The human error involved in choosing tie points as the point cloud has some noise at the edges of the building structures.

The effect of using distortion parameters obtained from the 2 scans, although not negligible, is not too highly pronounced. Only in one case (RMS residual for xp in scan 2), the value jumps by almost 45% (1.440 from 0.998) when we use the distortion parameters obtained from the other scan. This suggests that constant values for distortion parameters may be used but need to be checked consistently.

Table 4.1 Initial value of calibration parameters

Parameter	Value (scan 1)	Value (scan 2)
c_o(m)	[0.01, 0, 0.375]	[0.01, 0, 0.375]
p_0	[-0.677;67.217;-0.218]	[-0.298, 36.617, -0.851]
a_0	[-0.0102, 0.9999, -0.0088]	[-0.0084, 0.9994, -0.0334]
h_0	[3319.914, 1329.948, -11.432]	[3322.321, 1323.265, -43.366]
v_0	[-19.484, 1906.420, -3350.282]	[-15.336, 1823.312, -3396.248]

Table 4.2 Control Points for scan 1

	Image Coordinates (pixels)		Object Coordinates (m)		
	xp	Yp	X	Y	Z
1	1709	1911	6.197	55.411	0.112
2	336	968	-11.274	37.953	11.045
3	1957	1901	10.952	58.715	0.274
4	2258	1451	30.302	109.073	14.756
5	1880	886	12.559	75.554	23.134
6	1878	1255	13.467	82.047	16.014
7	2094	1892	20.239	88.995	0.453
8	2348	1228	36.021	117.893	23.711
9	2003	1676	17.44	86.979	5.987
10	1903	1775	14.953	87.52	3.493
11	2009	1352	17.681	87.002	14.354
12	2041	1405	19.171	90.207	13.501
13	943	1538	-7.457	65.239	7.447
14	1171	761	-2.852	63.292	21.943
15	801	1603	-8.94	57.076	5.412
16	1619	1500	6.303	72.514	8.854
17	1286	1105	-0.796	66.667	16.077
18	2325	799	34.677	115.341	38.26
19	1543	2415	3.829	60.543	-8.888
20	2254	2338	19.36	70.209	-8.937

Table 4.3 Control Points for scan 2

	Image Coordinates		Object Coordinates		
	xp	Yp	X	Y	Z
1	2413	1325	16.461	50.417	7.254
2	1315	1049	0.024	38.501	8.739
3	1414	2026	0.792	28.075	-1.639
4	697	689	-12.455	67.778	22.612
5	555	1086	-14.389	63.679	13.756
6	2413	1874	15.935	48.704	-0.961
7	2297	2113	13.311	45.442	-4.105
8	346	1904	-14.638	49.969	-1.276
9	586	1803	-9.348	42.873	0.174
10	909	2033	-7.432	60.348	-3.998
11	2129	1546	9.501	39.357	3.099
12	2331	1835	13.9	45.964	-0.354
13	810	1730	-6.186	41.045	1.094
14	1298	1459	-0.217	37.534	3.978
15	2130	1153	9.726	40.301	7.893
16	1107	1754	-2.688	43.035	0.773
17	1400	1608	0.682	28.003	1.826

Table 4.4 Camera model parameters

Parameter	Value (scan 1)	Value (scan 2)
c(m)	[-0.00805042, 0.799552, 0.3854579]	[-0.0013308, 0.8497070, 0.300866]
a(radians)	[0.0258054, 0.9993874, 0.0236395]	[0.000442, 0.999691, -0.024829]
h	[3451.5738, 1324.2397, 18.701148]	[3291.7308, 1316.9811, -46.0230]
v	[24.378744, 1897.1058, -3372.8594]	[-12.8117, 1791.2551, -3337.6421]
o	[0.0249488, 0.9994308, 0.0227091]	[0.0004532, 0.9996869, -0.0249463]
ρ0	-0.0002776	-.000271148
ρ1	-0.0164255	-0.005075091
ρ2	-0.0030774	-0.001171036

Table 4.5 Camera orientation in degrees

Orientation Axis	Scan 1	Scan 2
X	88.52129534	89.97467526
Y	2.005618374	1.424387172
Z	88.64543024	91.42274312

Table 4.6 Control point residuals for scan1 (in pixels)

	Scan 1 (distortion set 1)		Scan 1 (distortion set 2)	
	dxp	dyp	dxp	dyp
1	3.18	-1.07	-3.073	1.114
2	-0.19	1.59	-2.144	-3.457
3	1.41	0.95	-1.105	-0.910
4	-0.13	1.67	1.085	-2.088
5	-0.18	-2.46	0.822	1.204
6	1.43	-0.28	-1.065	-0.167
7	0.32	1.89	0.180	-1.843
8	0.09	-0.31	1.308	-0.571
9	1.21	-0.71	-0.840	0.620
10	-0.32	0.57	0.583	-0.597
11	1.02	-2.61	-0.522	2.228
12	1.44	-0.03	-0.916	-0.310
13	1.06	2.59	-1.328	-2.757
14	-3.43	2.03	3.094	-3.576
15	0.95	-1.65	-1.378	1.505
16	-0.76	-3.21	0.849	3.084
17	-0.18	-3.00	0.082	2.436
18	-1.00	3.15	2.998	-5.390
19	-2.20	0.78	2.295	-0.408
20	-3.73	0.12	4.806	0.530

Table 4.7 Control point residuals for scan2 (in pixels)

	Scan 2 (distortion set 2)		Scan 2 (distortion set 1)	
	Dxp	Dyp	Dxp	Dyp
1	1.25	0.95	-3.282	0.066
2	-1.61	-0.68	1.617	1.490
3	-0.09	0.29	0.065	-0.338
4	1.28	0.96	0.084	1.627
5	-1.98	-0.11	3.150	1.324
6	0.45	-0.07	-2.122	0.073
7	-1.48	0.73	0.179	-1.049
8	0.40	0.78	-0.454	-0.720
9	0.61	-1.79	-0.006	1.856
10	1.04	1.91	-0.857	-1.989
11	-0.87	-2.79	0.019	3.138
12	0.014	-0.43	-1.374	0.482
13	-0.37	1.11	0.650	-1.032
14	1.35	-1.90	-1.342	2.087
15	0.12	1.04	-1.350	0.040
16	-0.51	-1.80	0.583	1.839
17	0.40	1.79	-0.429	-1.711

Table 4.8 RMSE values for control point residuals

RMSE parameter	Scan 1 (D1)	Scan1 (D2)	Scan 2 (D2)	Scan 2 (D1)
RMSE dxp (pixels)	1.635	1.917	0.998	1.440
RMSE dyp (pixels)	1.851	2.202	1.349	1.487

Figure 4.1 Terrestrial Mapping System consisting of the laser scanner and the digital camera

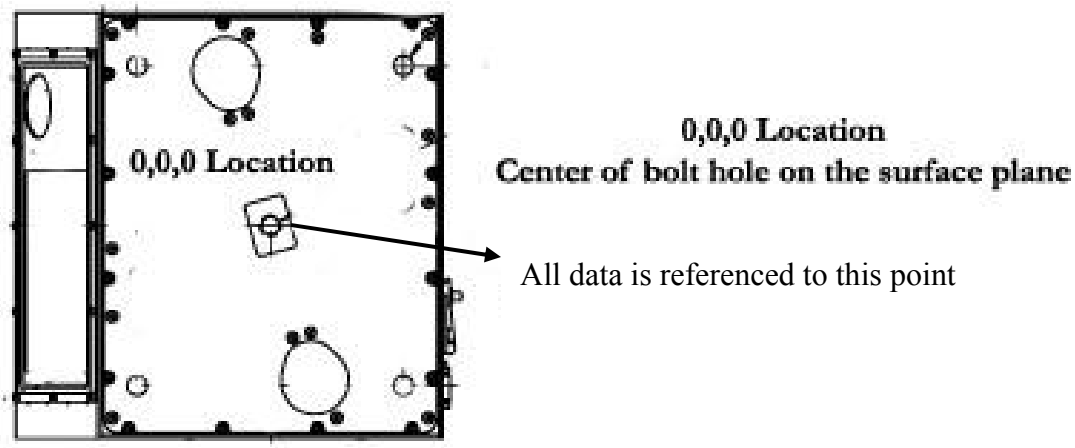

Figure 4.2 Point of origin for the laser data (ILRIS Product Manual)

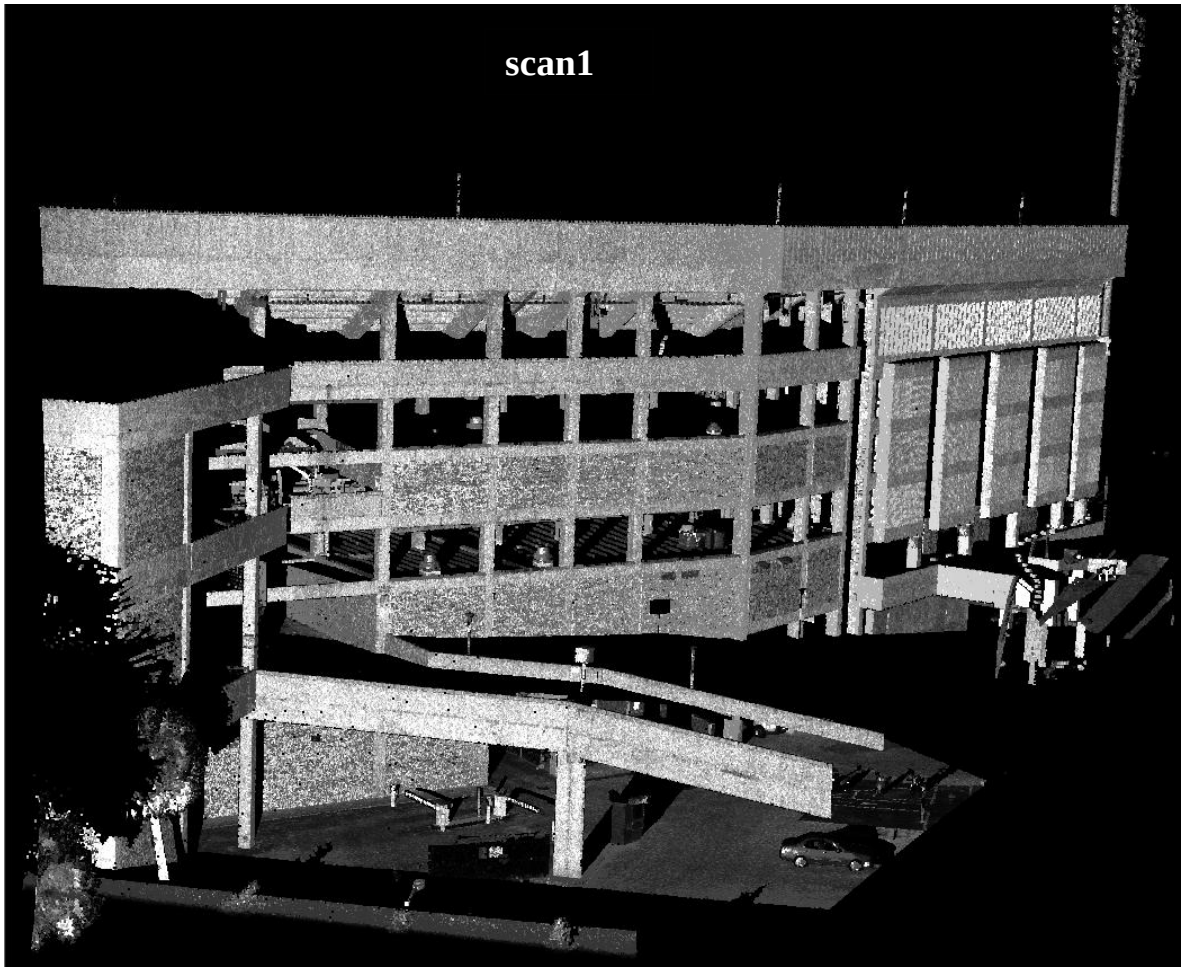

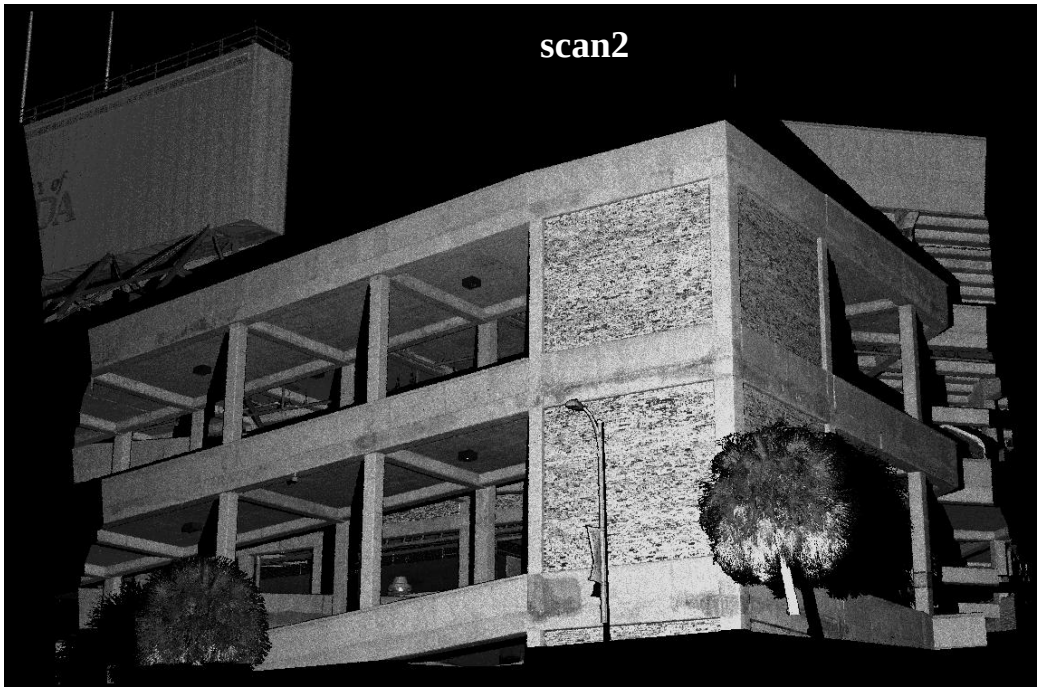

Figure 4.3 Point cloud with points color coded with intensity

Figure 4.4 Scan1 mage showing tie points

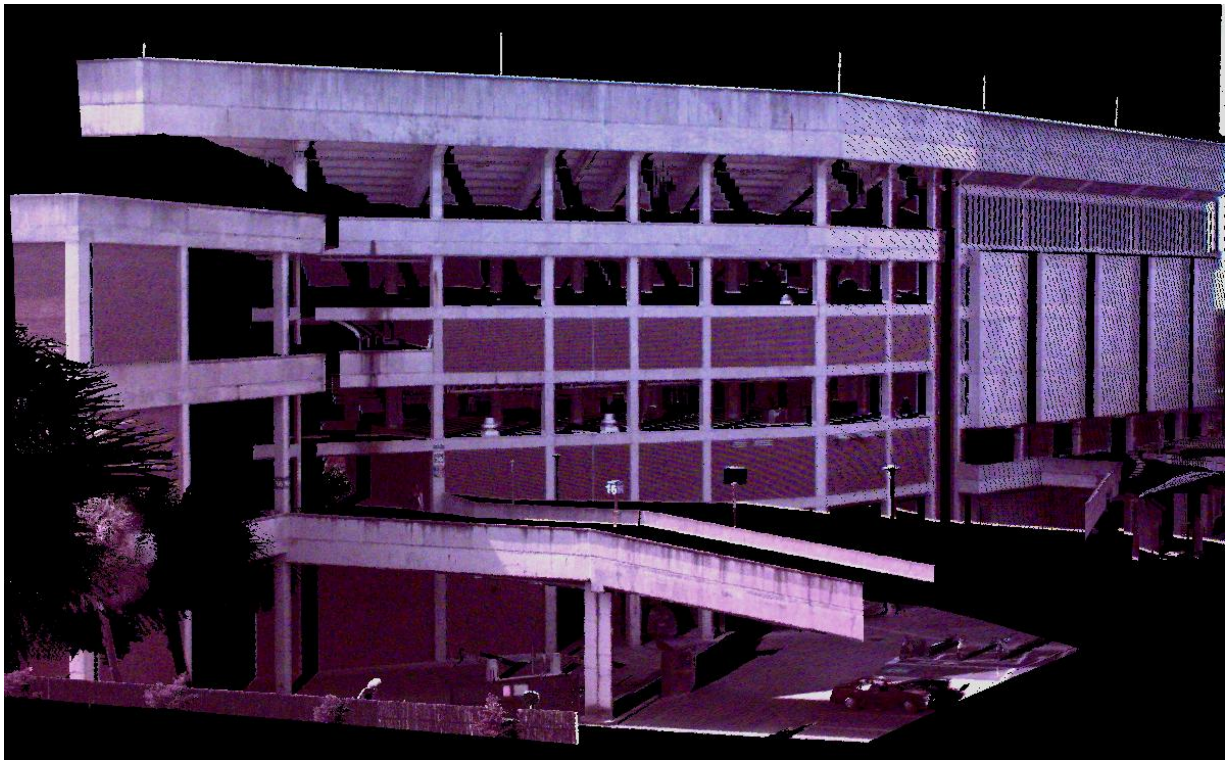

Figure 4.5 Laser point cloud color coded by RGB values obtained from the internal camera of the ILRIS

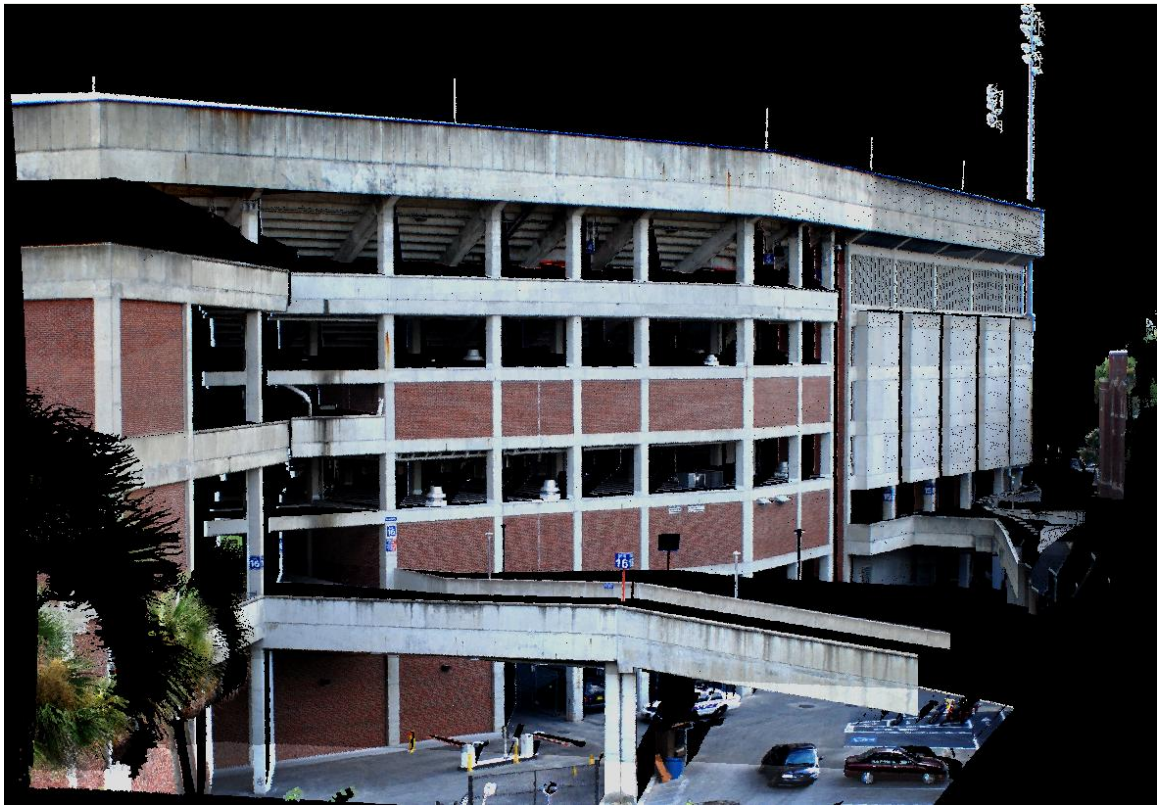

Figure 4.6 Laser point cloud color coded by RGB values obtained from external camera (scan 1)

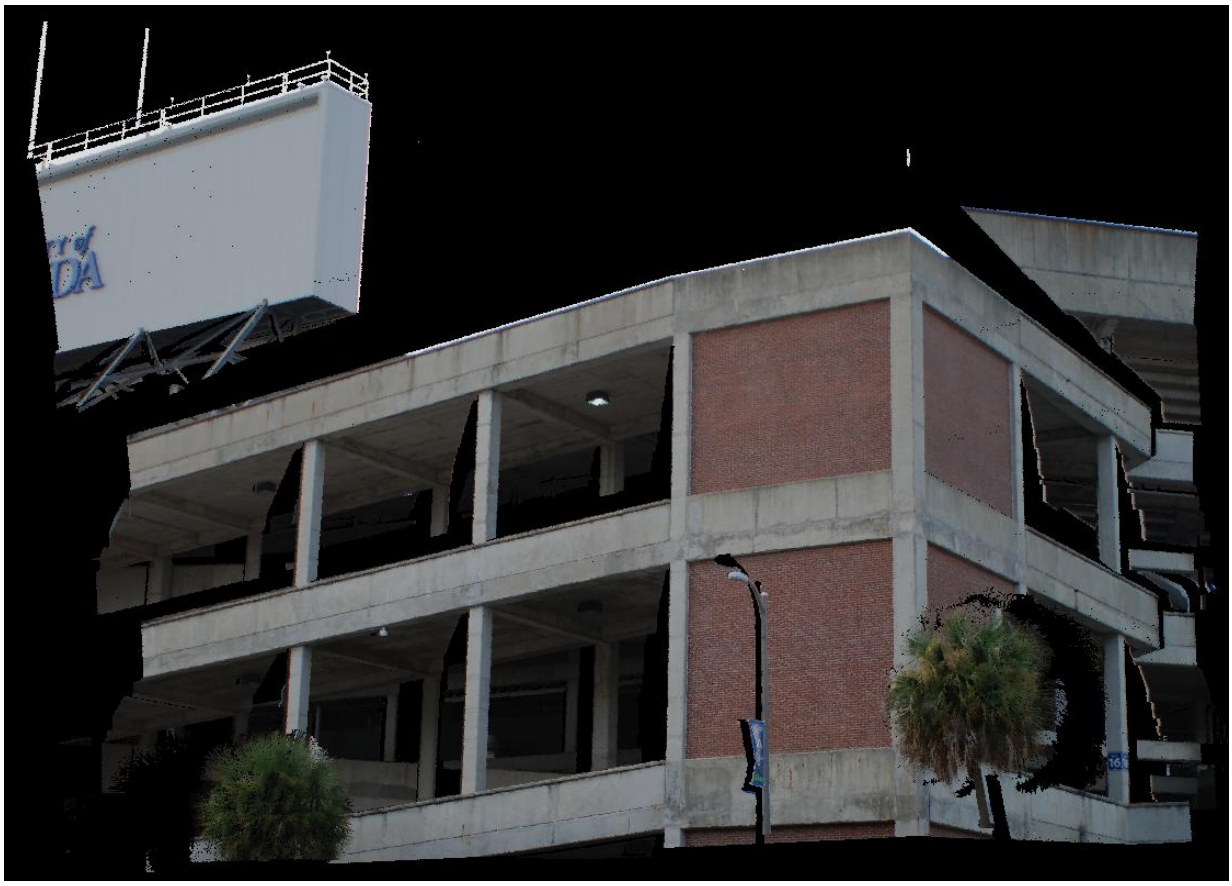

Figure 4.7 Laser point cloud color coded by RGB values obtained from external camera (scan 2)

CHAPTER 5
AIRBORNE CAMERA CALIBRATION

The airborne mapping system at UF consists of the ALTM 1233 laser scanning system and the MS4100 camera mounted on a twin engine Cessna airplane (Figure 5.1).

Study Area

Data was collected over the Oaks mall located in the west of the city of Gainesville (Figure 5.2), Florida on February 19, 2007. Flight was conducted over the parking lot so as to have clear road markings to obtain good tie points. The calibration field was about 375m x 350m in dimensions.

There were a total of 4 flight lines and 25 images (Table 5.1). The location of the study area showing the flight lines is shown in figure 5.3. The flight lines were designed keeping in mind the requirements for convergent network geometry

Calibration Data

The data obtained from the camera consisted of the images and the timestamps of each image in GPS time, up to a precision of nearest millisecond. The images were obtained at an interval of one second and the overlap between the images ranges from 45% to 80%. The trajectory information consisting of the position and the orientation of the airplane was obtained by post processing the GPS data to obtain differential GPS data (DGPS). This was then integrated with the IMU data and smoothened through a Kalman filter. POSPac software (Applanix, USA) was used to carry out these processes.

Initial Exterior and Interior Orientation

Exterior orientation elements required for calibration are the positional offsets between the reference points of the camera and the laser system. These are required as the trajectory obtained represents the position and orientation information in reference to the LIDAR system. They

were measured with the position of camera as origin and the positive X being forward (direction of flight), positive Z being skyward and positive Y to the right completing the right hand system. The values of these lever offsets are kept constant throughout the calibration process:

The initial values for the angular misalignment between the camera and the IMU were assumed to be zero.

The interior orientation parameters were obtained in 2005 from camera calibration carried out by USGS. However, when these values were used, the results obtained were inconsistent and out of acceptable limits. The reason for the same was not very clear and hence they were discarded. The interior orientation parameters were also determined with the self calibrating bundle adjustment.

The image position and orientation were extracted from the trajectory using the timestamps (Table 5.3). This was done by importing the image information and the trajectory to Terraphoto image processing software (developed and distributed by Terrasolid, Finland), where the position and orientation information for each image was interpolated from the trajectory file.

LIDAR Data

LIDAR data in the form of point cloud consisting of 746,223 points was collected simultaneously with the aerial images. The point density was about 5.6 points per square meter.

Tie Points and Ground Control

21 tie points and 5 ground control points were used for the calibration. Each image had at least 8 tie points and the average point count per image was 10.4. The distribution and location of the tie points (Table 5.5) and the ground control points (Table 5.4) are shown in figure 5.6 and 5.7. The ground control points were obtained from the intensity image (figure 5.5).

Using the initial orientation information of each image, ground coordinates were calculated for each tie point in each image. The average value of X and Y for each tie point was used as

initial value in the bundle adjustment. The Z coordinate for each point was obtained from the digital surface model created using the LIDAR point cloud.

Ground Truth Using GPS

The geodetic coordinates of the 21 tie points and the 5 control points were determined by carrying out a GPS survey over the study area. These positions were used as ground truth for comparison with the coordinates derived from georeferenced images. The procedure followed was that of a stop and go kinematic survey. The main reference base station was set up in the study area and collected data for 3 hours. Its purpose was to obtain short baselines (< 250m) with respect to the rover stations. A second base station, a CORS (Continually Operating Reference Stations), located at the Gainesville Regional Airport was also used. The antenna used for the base station was a dual frequency (L1/L2) ASHTECH manufactured Chokering 700936 Rev D antenna. For the roving station, the antenna used was dual frequency ASHTECH manufactured ASH700700.C antenna. The receiver make and model used for both the base and the rover stations was an ASHTECH Z-Xtreme receiver. It is dual frequency (L1/L2), carrier phase, 12 channel, geodetic quality receiver.

The data was post processed for differential positioning using carrier phase tracking in the Ashtech Office Suite (AOS) software. The software reduces the GPS observations files performing a series of Least Squares vector distance calculations between the stations to derive the final stations coordinates. The positions obtained are given in Table 5.6. The expected values of accuracy for the survey practice followed and the carrier phase differential post processing is less than 5 cm (USACE, 2003)

Calibration Results

The self calibrating bundle adjustment was carried out in TerraPhoto using the above data. The external misalignments as well as the internal orientation parameters were determined and are presented in Table 5.10. To access the accuracy, the images were georeferenced in X and Y using the obtained calibration parameters and the position of tie points as well as the control points was calculated (Table 5.7) and compared to the GPS surveyed ground truths (Table 5.8). The LIDAR surface was overlaid with georeferenced images and the Z coordinate values were obtained for the control points.

The position of the tie points was calculated for each image and then averaged. The standard deviation for each tie points was also calculated as an indication for the mismatch between the images. The standard deviations varied between 10 and 40 cm.

Residuals were calculated for these mean coordinates from the ground truth values. The maximum residual in X was -0.359m and in Y was -0.366m. The various sources of error are:

- Image pixel resolution: The images were taken at different altitudes to have a convergent geometry for better determinability of the focal length. The image resolution therefore varied from 15 cm for images taken at 650m to 35 cm for images taken at 900m altitude. This would result in higher error in the chosen tie points for the lower resolution images as the error involved in the geodetic coordinate of a pixel is proportional to the image pixel resolution.
- Error in control points chosen from LIDAR intensity image: The LIDAR intensity image was used for providing the few control points. Therefore any error in LIDAR data is also introduced in the calibration.
- Human error in choosing tie points accurately: Misplacement of a tie point by a couple of pixels translates to an error ranging from 30 cm to 70 cm (image pixel resolutions ranging from 15 cm to 35 cm).
- Uncertainty in the coordinates of the ground truths because of various sources of error in GPS as discussed in the USACE (Unites States Army Corps of Engineers), NAVSTAR GPS ground surveying engineering manual

The values of residuals are equivalent to about 1.5 pixels on the image, scaled at an average flying height of 750m. The root mean square error (RMSE) values were calculated for the residuals, which lied between 20-30cms. This is also equivalent to about 1-2 image pixels (scaled at 750m). These results indicate that the errors are within acceptable limits for the application of overlaying the georeferenced imagery and LIDAR point cloud (or the digital elevation model obtained from the point cloud). Figure 5.8 shows the georeferenced imagery overlaid with the point cloud color coded with elevation. Near the edge of the building, the good match between the imagery and the point cloud is evident.

Table 5.1 Flight line information

Line No	Direction	Elevation (m)	No. of images
1	N – S	610	8
2	E – W	620	6
3	NW – SE	780	5
4	SE – NW	906	6

Table 5.2 Lever arms between the laser and the camera

X Lever arm(m)	-0.184
Y Lever arm(m)	0.019
Z Lever arm(m)	0.075

Table 5.3 Initial image data as obtained from trajectory file

Image(m)	Easting(m)	Northing(m)	Elevation(m)	Heading(º)	Roll(º)	Pitch(º)
20071.tif	363539.239	3281072.783	610.258	1.51164	1.32967	3.70937
20072.tif	363539.711	3281118.359	610.833	1.62677	0.9302	3.52244
20073.tif	363540.22	3281163.873	611.498	1.78747	0.88235	3.36686
20074.tif	363540.765	3281209.313	612.254	1.72788	0.87308	3.16959
20075.tif	363541.331	3281254.667	613.062	1.63111	0.67809	2.92838
20076.tif	363541.879	3281299.932	613.904	1.64153	0.47138	2.7199
20077.tif	363542.372	3281345.105	614.765	1.60359	0.21121	2.4738
20078.tif	363542.779	3281390.185	615.618	1.70767	0.13646	2.22879
40052.tif	363673.16	3281180.328	620.369	-85.04473	0.59574	1.85774
40053.tif	363614.636	3281178.969	620.266	-84.85696	0.16935	1.42818
40054.tif	363556.006	3281177.578	620.155	-84.79359	0.00001	1.06588
40055.tif	363497.266	3281176.14	620.061	-84.76166	0.06468	0.65269
40056.tif	363438.419	3281174.72	619.948	-83.46022	0.95124	0.2977
40057.tif	363379.487	3281173.58	619.841	-82.97238	1.41948	0.01577
50056.tif	363465.92	3281388.218	772.047	131.35963	0.33675	6.28305
50057.tif	363500.294	3281343.97	774.356	131.6376	1.27795	6.00698
50058.tif	363534.856	3281299.671	776.674	131.67739	1.89909	5.71967
50059.tif	363569.53	3281255.249	779.009	131.79372	1.83026	5.4413
50060.tif	363604.318	3281210.713	781.352	132.05705	1.87282	5.15806
60070.tif	363662.081	3281143.366	906.768	-32.83432	1.03541	1.33601
60071.tif	363627.495	3281187.821	906.591	-32.68246	1.17407	1.29418
60072.tif	363593.063	3281232.391	906.607	-32.55669	1.16715	1.26089
60073.tif	363558.799	3281277.04	906.763	-32.29035	0.68233	0.8148
60074.tif	363524.644	3281321.756	906.705	-32.17591	0.47473	0.28121
60075.tif	363490.538	3281366.562	906.366	-32.26497	0.05857	-0.02744

Table 5.4 Ground control points

Point No.	X(m)	Y(m)	Z(m)
22	363434.2570	3281124.2750	-1.4000
23	363473.9710	3281158.7450	-2.5700
24	363534.1710	3281154.8450	-3.4000
25	363572.9050	3281140.8650	-4.0500
26	363591.2770	3281107.5760	-4.3000

Table 5.5 Initial coordinates for each tie point

Tiepoints	X(m)	StdX(m)	Y(m)	StdY(m)	Z(obtained from LIDAR Surface)
1	363531.804	1.817	3281194.443	6.049	-3.284
2	363440.286	6.355	3281127.506	8.626	-1.615
3	363369.863	6.580	3281285.467	9.486	-3.216
4	363449.257	5.909	3281215.742	8.984	-2.701
5	363417.374	5.961	3281243.104	8.999	-3.449
6	363635.068	1.577	3281098.324	7.071	-4.887
7	363429.035	6.212	3281159.818	8.629	-1.291
8	363475.455	3.744	3281180.688	6.991	-2.414
9	363572.574	1.880	3281373.231	5.165	2.737
10	363589.406	1.920	3281326.842	5.642	-0.717
11	363578.609	1.879	3281256.823	5.631	-2.29
12	363491.439	1.725	3281353.426	3.919	1.974
13	363580.878	1.632	3281459.991	3.713	1.395
14	363375.933	6.529	3281313.127	9.096	-3.667
15	363581.268	0.712	3281516.290	3.080	0.91
16	363653.528	2.371	3281339.257	5.473	-3.96
17	363573.191	1.759	3281125.164	6.802	-3.985
18	363641.140	2.149	3281233.807	6.781	-4.75
19	363534.868	1.802	3281122.679	6.196	-3.405
20	363645.286	3.195	3281195.712	7.074	-5.083
21	363676.255	2.028	3281419.934	6.207	-3.03
	MEAN	**3.225**	**MEAN**	**6.648**	

Table 5.6 Control Points obtained from GPS survey

Easting (m)	Northing(m)	Elevation (m)
363530.057	3281182.043	-3.718
363440.115	3281110.729	-1.792
363368.851	3281272.928	-3.375
363449.464	3281201.388	-2.352
363417.082	3281229.519	-3.17
363634.394	3281083.505	-5.163
363428.708	3281143.614	-1.569
363474.181	3281167.159	-2.859
363571.622	3281364.48	0.132
363588.096	3281315.181	-1.401
363577.316	3281243.937	-2.958
363489.713	3281344.937	1.159
363579.25	3281452.49	1.291
363374.711	3281300.603	-3.993
363580.341	3281510.422	0.632
363652.841	3281328.017	-4.328
363571.852	3281110.708	-4.329
363640.521	3281221.841	-5.218
363532.961	3281108.765	-3.706
363643.531	3281183.567	-5.37
363674.834	3281408.853	-3.461
363434.283	3281124.537	-1.633
363474.033	3281159.04	-2.893
363534.152	3281155.076	-3.623
363572.696	3281140.656	-4.404
363591.055	3281107.576	-4.612

Table 5.7 Orientation parameters from Self calibrating bundle adjustment

Parameter		Value
Heading (degrees)		-0.1439
Roll (degrees)		-0.9812
Pitch (degrees)		-1.7004
Focal length		24.7124 (mm)
Principle point coordinates	xp	0.4347 (mm)
	yp	0.5131 (mm)
Radial Distortion Parameters	K1	-7.02502×10^{-5}
	K2	-6.71944×10^{-6}
	K3	7.25511×10^{-8}
Decentering Distortion Parameters	P1	-4.065754×10^{-4}
	P2	-4.618851×10^{-4}

Table 5.8 Average geodetic position derived from georeferenced imagery for each tie point with standard deviations

Point No.	Easting(X) (m)	σ_x (m)	Northing(Y) (m)	σ_y (m)
1	363529.972	0.138	3281181.904	0.147
2	363440.102	0.108	3281110.497	0.161
3	363368.517	0.168	3281272.562	0.191
4	363449.314	0.134	3281201.08	0.124
5	363416.769	0.131	3281229.187	0.153
6	363634.611	0.133	3281083.623	0.142
7	363428.582	0.165	3281143.307	0.143
8	363474.074	0.128	3281166.911	0.119
9	363571.263	0.175	3281364.567	0.167
10	363587.792	0.141	3281315.236	0.184
11	363577.021	0.294	3281244.738	0.198
12	363489.459	0.165	3281344.683	0.216
13	363579.473	0.141	3281452.646	0.176
14	363374.574	0.154	3281300.283	0.157
15	363580.21	0.175	3281510.55	0.183
16	363652.948	0.193	3281328.329	0.243
17	363572.016	0.103	3281110.682	0.127
18	363640.335	0.155	3281221.574	0.118
19	363533.101	0.114	3281108.572	0.132
20	363643.738	0.165	3281183.352	0.221
21	363675.135	0.452	3281409.07	0.278
22	363434.257	0.125	3281124.275	0.153
23	363473.971	0.116	3281158.745	0.107
24	363534.171	0.201	3281154.845	0.262
25	363572.905	0.244	3281140.865	0.281
26	363591.277	0.102	3281107.576	0.113
	Mean	**0.166**	**Mean**	**0.173**

Table 5.9 Residuals obtained from comparison of derived geodetic coordinates with GPS surveyed ground truths

Point No.	dX (m)	dY (m)
1	-0.085	-0.139
2	-0.013	-0.232
3	-0.334	-0.366
4	-0.15	-0.308
5	-0.313	-0.332
6	0.217	0.118
7	-0.126	-0.307
8	-0.107	-0.248
9	-0.359	0.087
10	-0.304	0.055
11	-0.295	0.801
12	-0.254	-0.254
13	0.223	0.156
14	-0.137	-0.32
15	-0.131	0.128
16	0.107	0.312
17	0.164	-0.026
18	-0.186	-0.267
19	0.14	-0.193
20	0.207	-0.215
21	0.301	0.217
22	-0.026	-0.262
23	-0.062	-0.295
24	0.019	-0.231
25	0.209	0.209
26	0.222	0
RMSE	**0.205**	**0.277**
MEAN	**-0.0412**	**-0.0635**

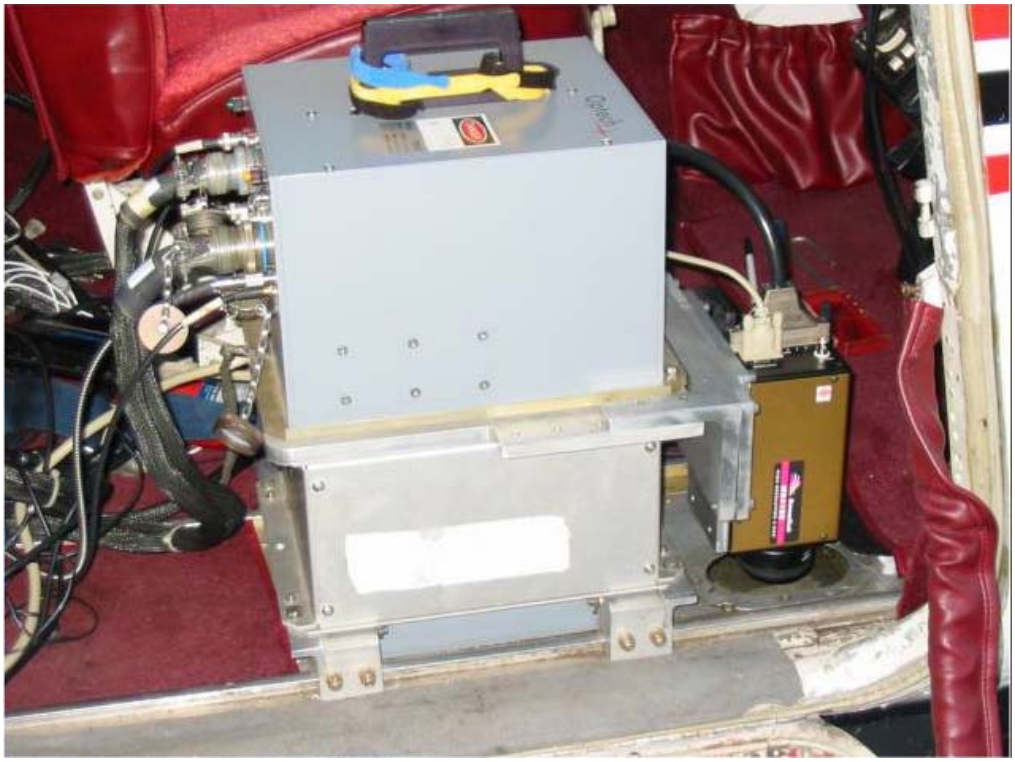

Figure 5.1 Airborne Mapping System showing the laser head and the camera

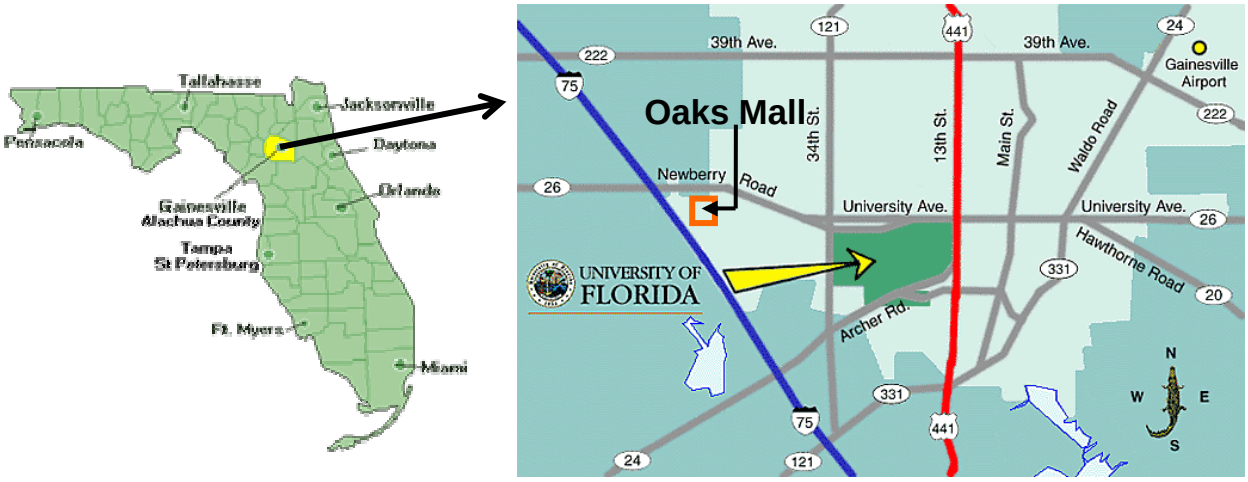

Figure 5.2 Location of the study area

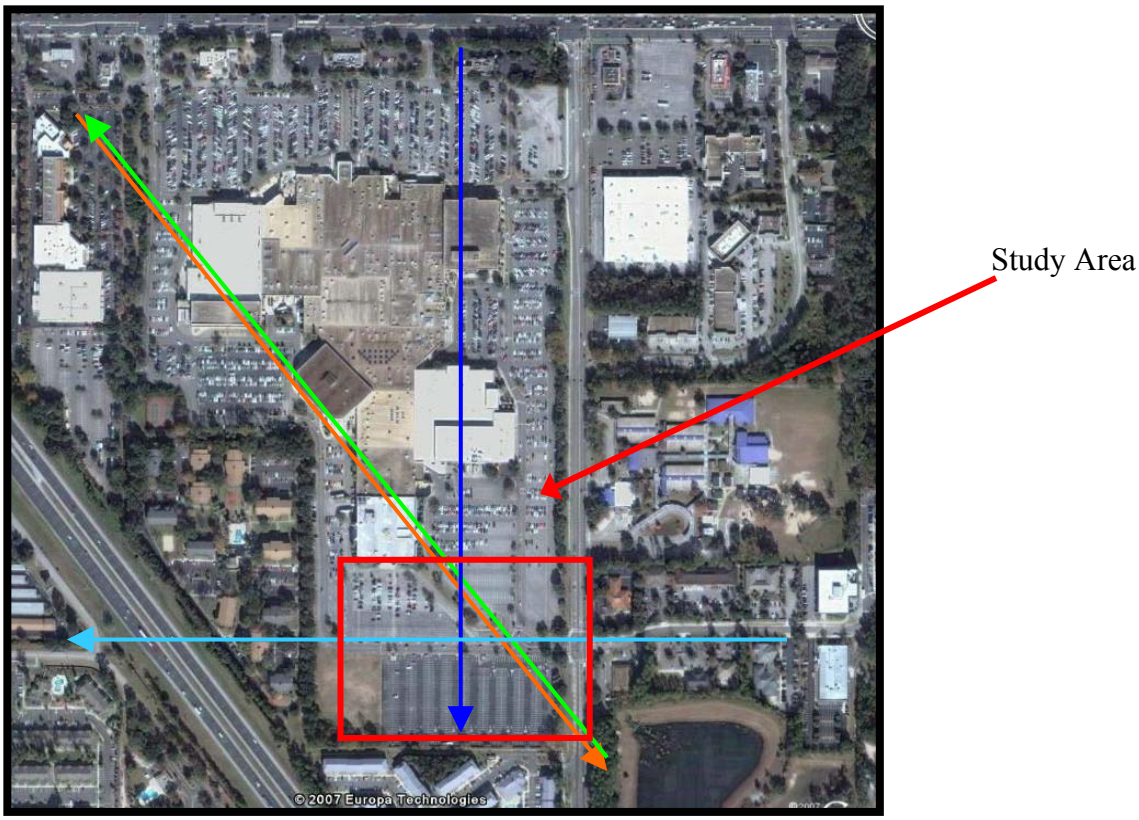

Figure 5.3 Study area showing flight lines location and orientation

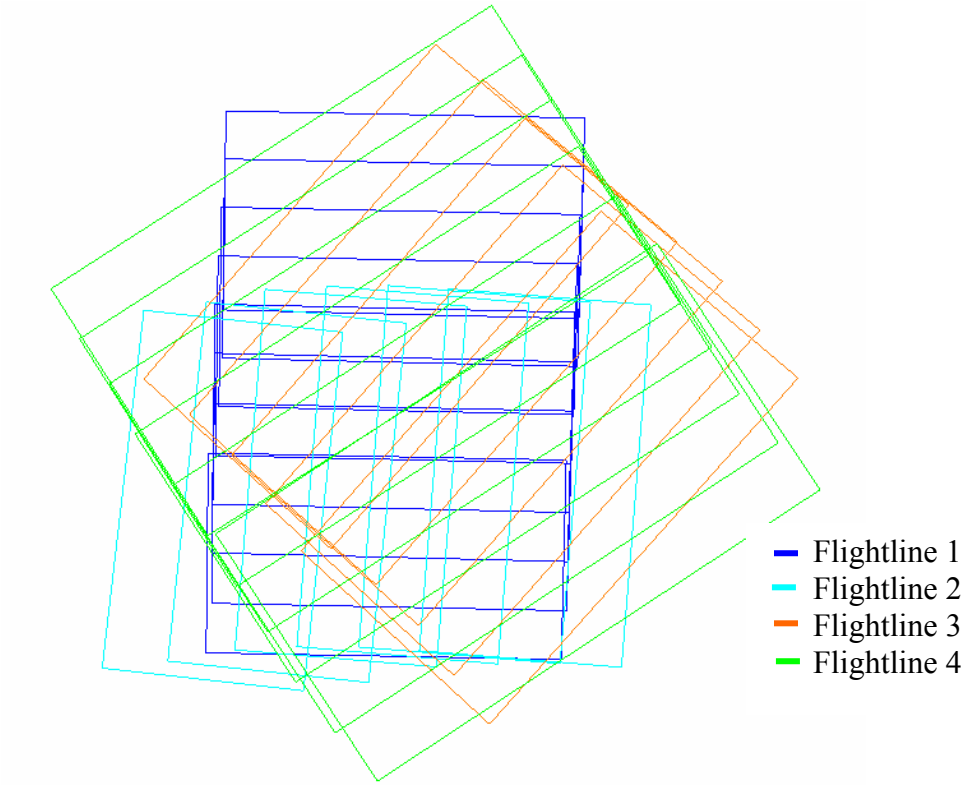

Figure 5.4 Image footprints colour coded by flight lines

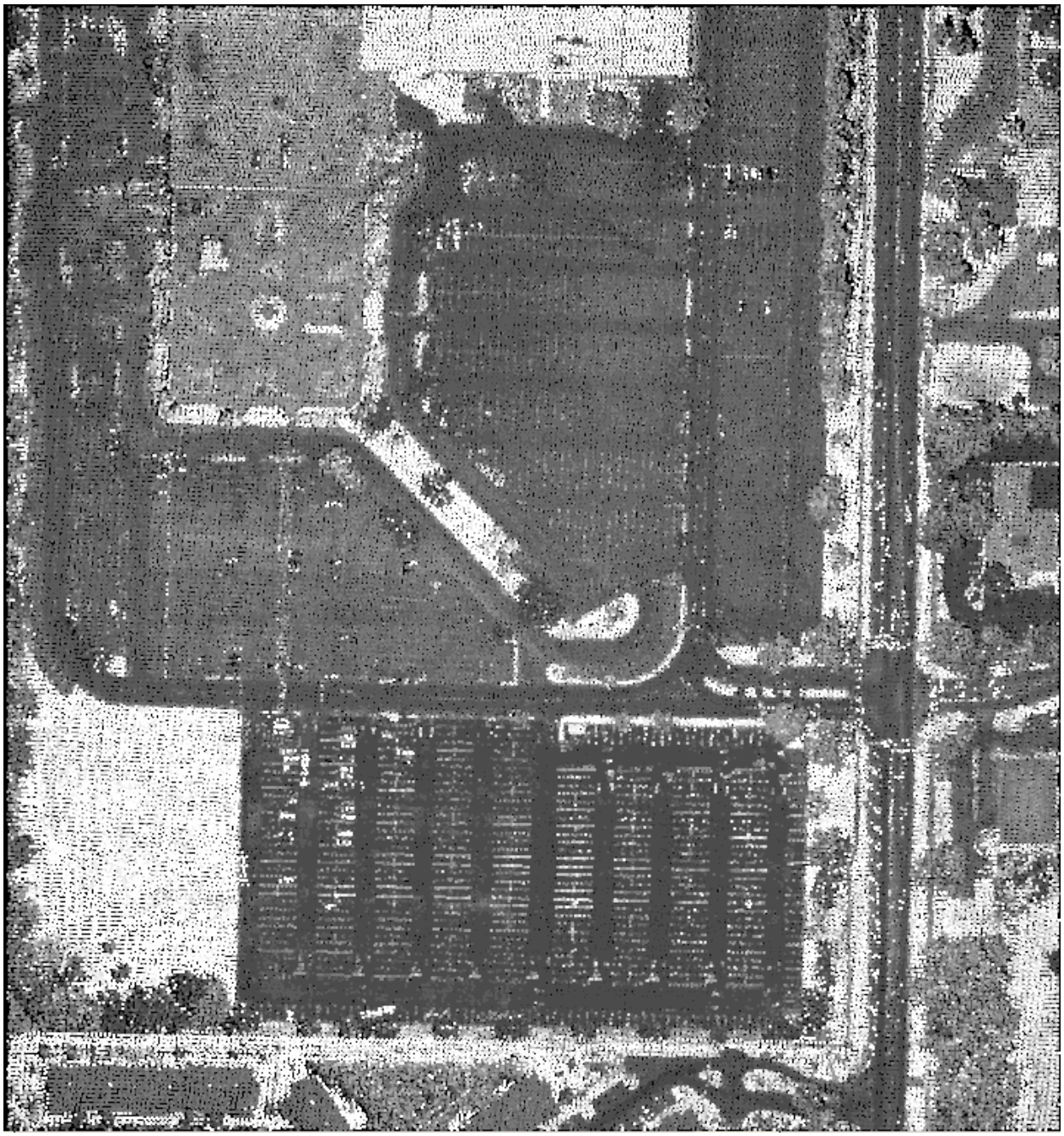

Figure 5.5 Intensity image from LIDAR data

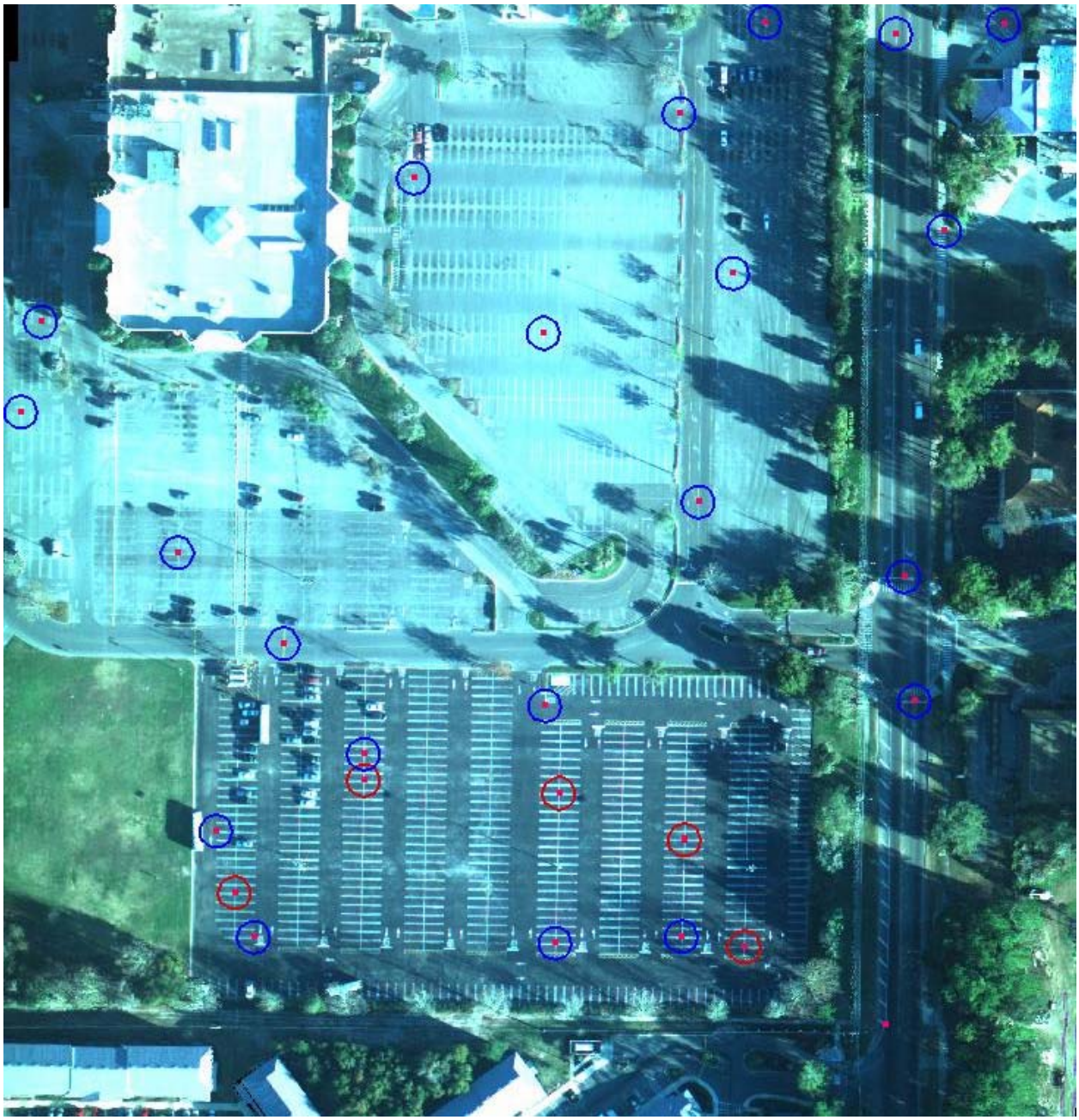

Figure 5.6 Tie points (blue circle) and Ground control points (red circle)

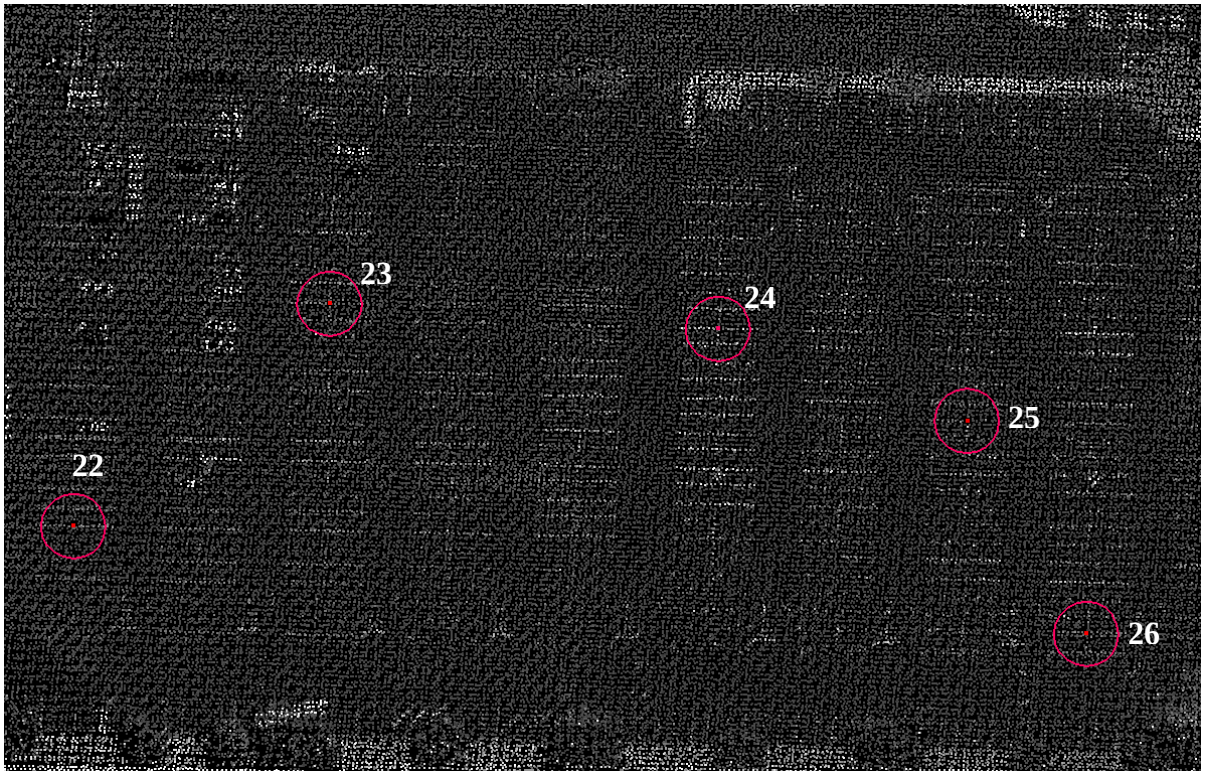

Figure 5.7 Intensity image with ground control points

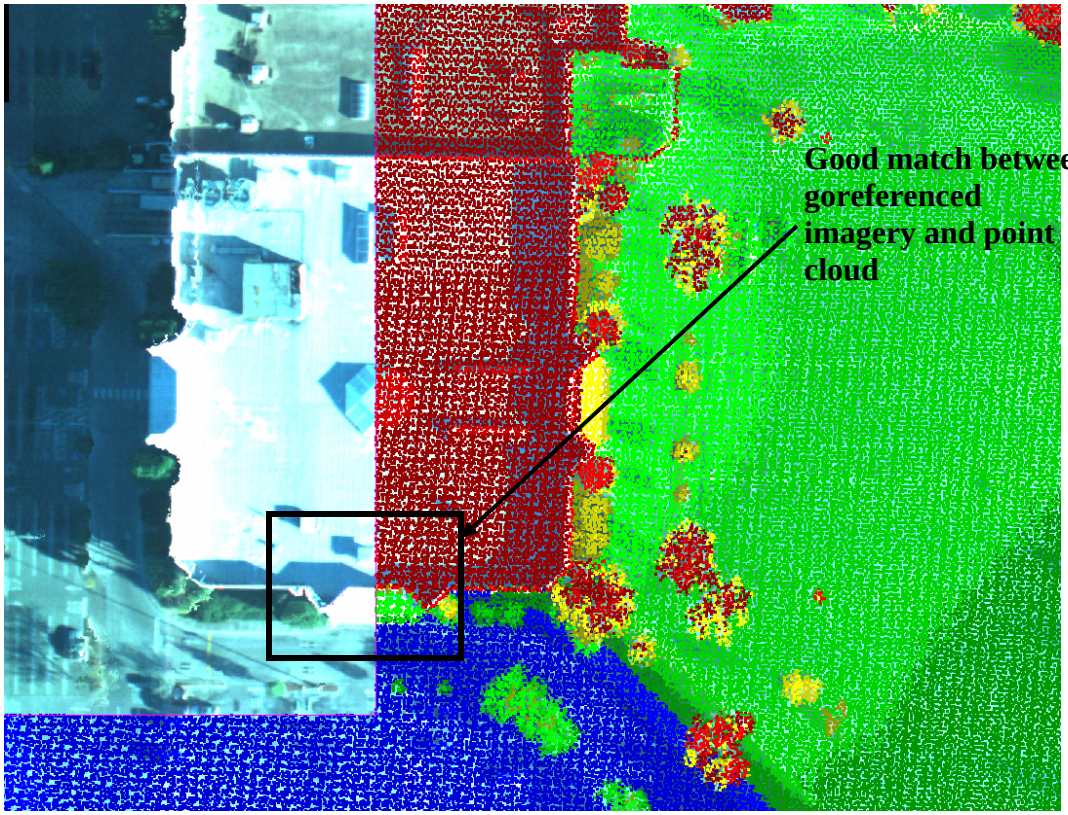

Figure 5.8 Georeferenced imagery overlaid with point cloud color coded with elevation

CHAPTER 6
CONCLUSION

An effort was made here to demonstrate the procedure of calibration of cameras using LIDAR data for both terrestrial as well as aerial applications. The perspective collineation camera model provided the basic mathematical model for carrying out the calibration.

For the terrestrial camera, LIDAR provided a three dimensional calibration field and the calibration procedure was based on the space resection principal. The root mean square error for control point residuals lied in the range of 1-2 pixels, maximum being 2.2. Good agreement between the laser data and the referenced images indicated successful calibration of the camera. Two scans were done on different days to assess the stability and repeatability of the parameters. Although the interior distortion parameters were consistent, the external parameters varied by few centimeters for the translational offsets and by a couple of degrees in angular orientation. This is attributed to the fact that the mount for the camera is not rigid enough so as to ensure repeatable relative orientation between the camera and the laser system. Therefore the present system would need to be calibrated every time the camera is taken off the laser system. An extra day for processing calibration data would be needed for each day of survey work as the camera would be required to be taken off for storing and transporting the laser system safely. The mount is one aspect that needs to be improved so as to provide more repeatable values for the external parameters, and hence rendering the system much more practically useful

For the aerial cameras, LIDAR data provided an intensity image for selecting ground control points (without any external setup) and also a surface model which was used to give a constant scaling factor for the transformation as well as elevation values to the georeferenced imagery. Self calibration bundle adjustment was carried out for the determination of orientation parameters. The residual RMSE values for the tie points were 20 cm in X and 28cm in Y. These

values indicate good agreement between the georeferenced images and the ground truths. Moreover, with the improved accuracy of airborne LIDAR data and the pulse frequencies reaching high numbers like 166kHz for the latest Optech GEMINI system, results obtained from LIDAR aided camera calibration can be expected to improve. Laser data used for doing the calibration in the study was collected using a 33 kHz pulse frequency laser system. The point density obtained after multiple overlaps was about 5 points per square meter. As seen in the figure 5.5 the paint markings to be used as ground control are visible but faintly defined and hence affecting the accuracy with which they can be marked. Using higher pulse frequency systems, better LIDAR density would lead to better control in choosing the GCPs and hence improved calibration.

APPENDIX A
CAMERA MODELS

Projective Model

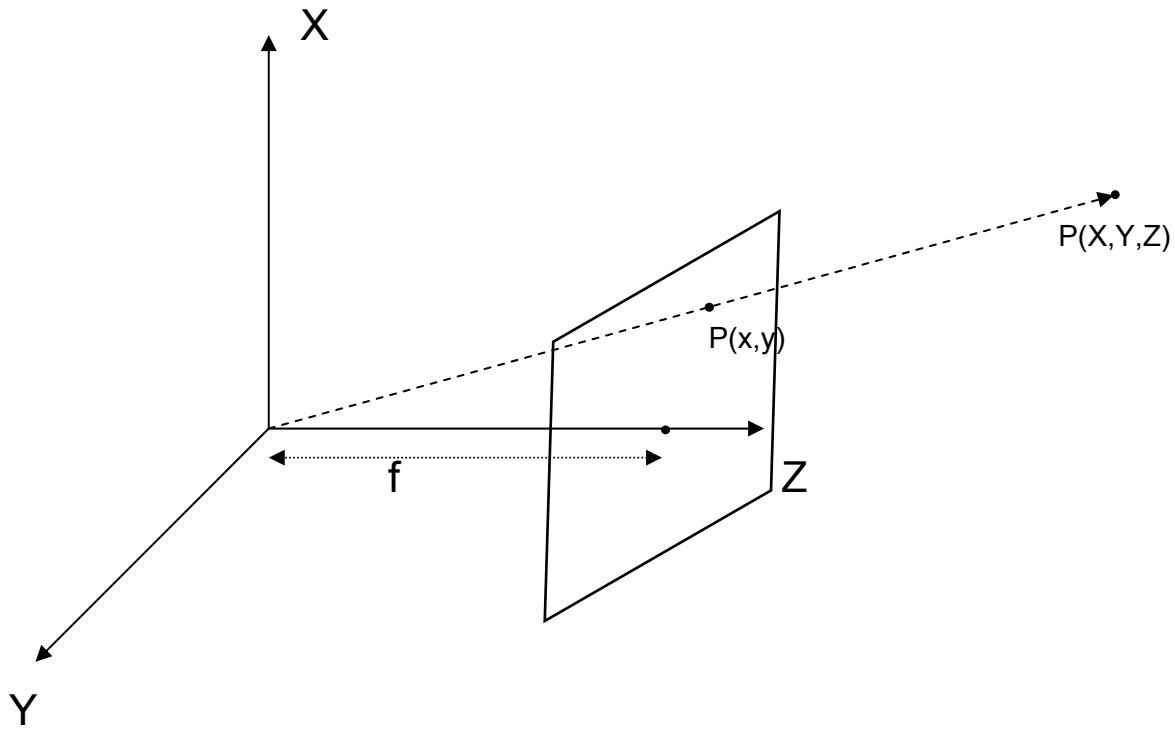

Figure A.1 Projective camera model using standard perspective projection

Let (x; y) be the 2D image coordinates of p and (X; Y; Z) the 3D coordinates of P. Now from the figure it can be seen

$$x = \frac{fX}{Z}$$

$$y = \frac{fY}{Z}$$

f = 1 can be assumed as different values of f just correspond to different scalings of the image such that $\begin{pmatrix} x \\ y \\ 1 \end{pmatrix}$ corresponds to $\begin{pmatrix} X \\ Y \\ Z \end{pmatrix}$.

In homogeneous coordinates, it can be written as:

$$\begin{pmatrix} x \\ y \\ 1 \end{pmatrix} \sim \begin{pmatrix} X \\ Y \\ Z \end{pmatrix} = \begin{pmatrix} 1 & 0 & 0 & 0 \\ 0 & 1 & 0 & 0 \\ 0 & 0 & 1 & 0 \end{pmatrix} \begin{pmatrix} X \\ Y \\ Z \\ 1 \end{pmatrix}$$

In real images, the origin of the image coordinates is not the principal point and the scaling along each image axis is different, so the image coordinates undergo a transformation described by the matrix K (interior camera parameters) as described above. Also, the world coordinate system does not usually coincide with the perspective reference frame, so a coordinate transformation is required given by matrix M. Finally we get:

$$\begin{pmatrix} x \\ y \\ 1 \end{pmatrix} = K \begin{pmatrix} 1 & 0 & 0 & 0 \\ 0 & 1 & 0 & 0 \\ 0 & 0 & 1 & 0 \end{pmatrix} M \begin{pmatrix} X \\ Y \\ Z \\ 1 \end{pmatrix}$$

Perspective Model

Consider figure A.2 shown below; the image coordinate system is parallel to the object mapping coordinate system. L is the exposure station or the perspective center with coordinates X_L, Y_L and Z_L in object mapping frame; Xo, Yo and Zo are the object coordinates in the mapping frame; x_a, y_a, z_a are the image coordinates in image frame;. From the similar triangles collinearity condition equations are as follows (Wolf & Dewitt, 2001):

$$\frac{x_a}{Xo - X_L} = \frac{y_a}{Yo - Y_L} = \frac{-z_a}{Zo - Z_L}$$

or $\quad x_a = \left(\frac{X_L - Xo}{Zo - Z_L} \right) z_a ; \quad y_a = \left(\frac{Y_L - Yo}{Zo - Z_L} \right) z_a \quad$ and $\; z_a = \left(\frac{Zo - Z_L}{Zo - Z_L} \right) z_a$

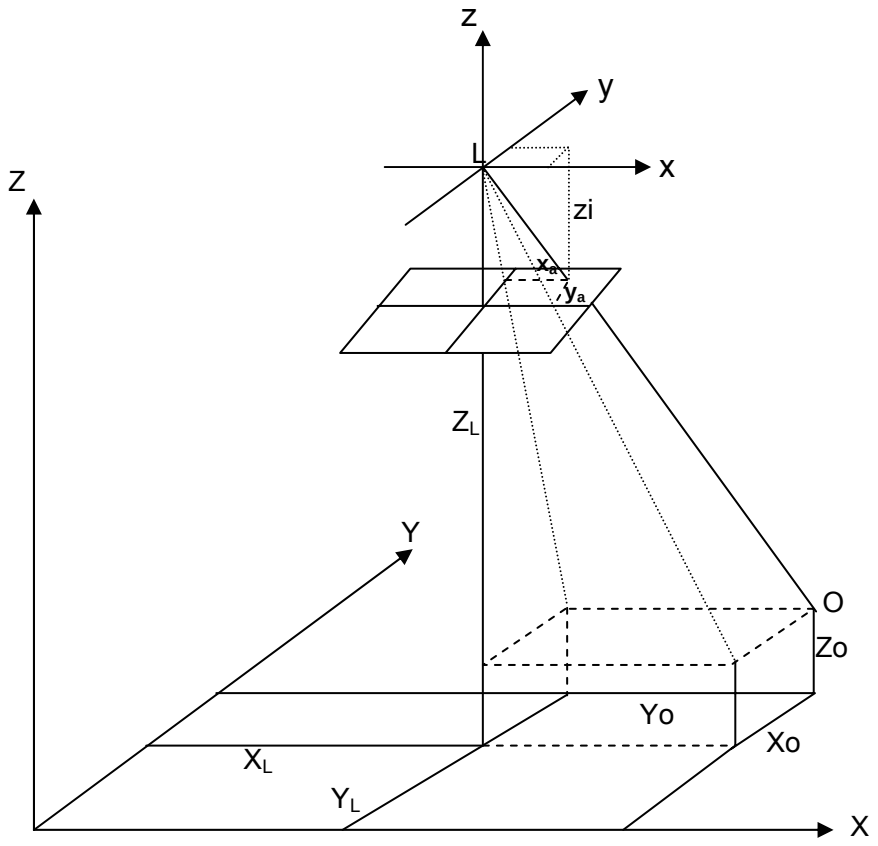

Figure A.2 Image coordinate system parallel to mapping coordinate system

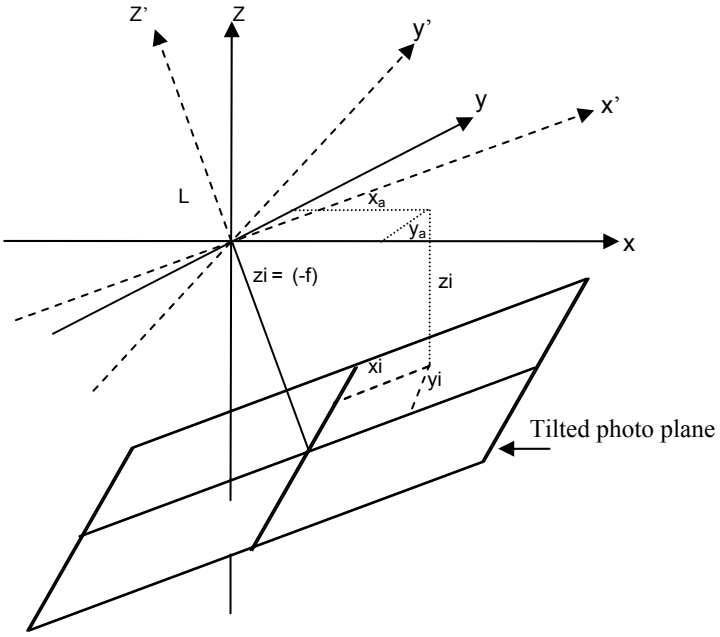

Figure A.3 Image coordinates transformation in the tilted photo plane

Now consider figure A.3 showing a tilted image. The relationship between the actual coordinates of the tilted image (xi, yi) and the image coordinates for the un-tilted image can be expressed as:

$xi = r_{11}x_a + r_{12}y_a + r_{13}z_a$

$yi = r_{21}x_a + r_{22}y_a + r_{23}z_a$

$zi = r_{31}x_a + r_{32}y_a + r_{33}z_a$

where r_{11}, r_{12}…….r_{ij} etc are the i_{th} and j_{th} terms of the rotation matrix defining rotation from the mapping coordinate system to tilted coordinate system of the exposure station. Substituting x_a,y_a and z_a we get

$$xi = r_{11}\left(\frac{X_L - Xo}{Zo - Z_L}\right)z_a + r_{12}\left(\frac{Y_L - Yo}{Zo - Z_L}\right)z_a + r_{13}\left(\frac{Zo - Z_L}{Zo - Z_L}\right)z_a \quad (1)$$

$$yi = r_{21}\left(\frac{X_L - Xo}{Zo - Z_L}\right)z_a + r_{22}\left(\frac{Y_L - Yo}{Zo - Z_L}\right)z_a + r_{23}\left(\frac{Zo - Z_L}{Zo - Z_L}\right)z_a \quad (2)$$

$$zi = r_{31}\left(\frac{X_L - Xo}{Zo - Z_L}\right)z_a + r_{32}\left(\frac{Y_L - Yo}{Zo - Z_L}\right)z_a + r_{33}\left(\frac{Zo - Z_L}{Zo - Z_L}\right)z_a \quad (3)$$

Now factor out z_a / (Zo - Z_L), divide equations (1) and (2) by equation (3) and replace zi by (-f) to obtain the following collinearity equations

$$xi = -f\left[\frac{r_{11}(X_L - Xo) + r_{12}(Y_L - Yo) + r_{13}(Z_L - Zo)}{r_{31}(X_L - Xo) + r_{32}(Y_L - Yo) + r_{33}(Z_L - Zo)}\right]$$

$$yi = -f\left[\frac{r_{21}(X_L - Xo) + r_{22}(Y_L - Yo) + r_{23}(Z_L - Zo)}{r_{31}(X_L - Xo) + r_{32}(Y_L - Yo) + r_{33}(Z_L - Zo)}\right]$$

f is the focal length of the camera.

APPENDIX B
IMAGING AND MAPPING SENSORS AT UF

Laser systems

University of Florida acquired its first airborne laser mapping system, Optech ALTM 1233 in 1998, in collaboration with the Florida International University (FIU) and created an Airborne Laser Swath Mapping (ALSM) research center. The System is operated on a Cessna 337 twin engine aircraft at an approximate altitude of about 600m and speed 60m/sec.

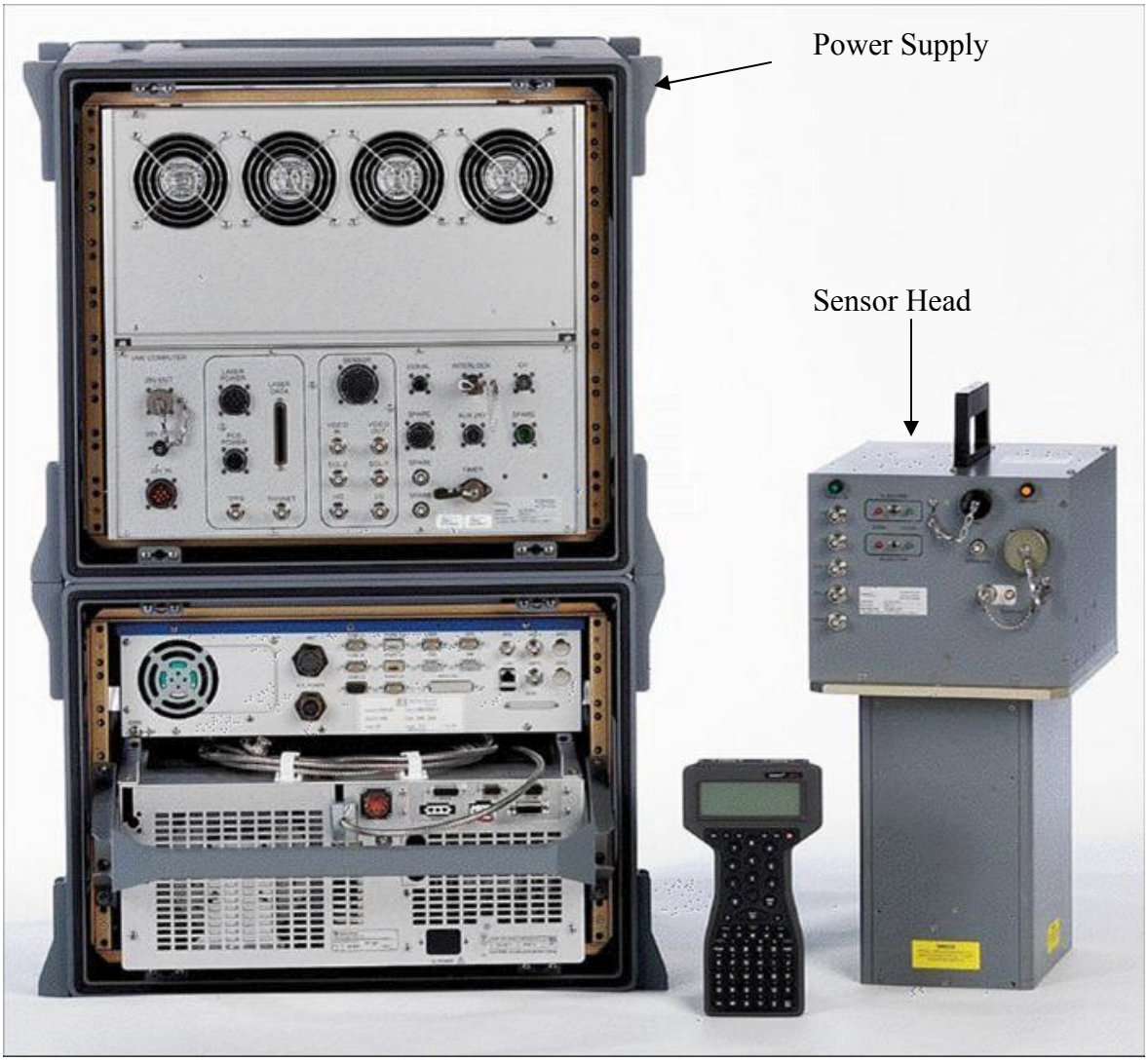

Figure B.1 ALTM 1233 Airborne laser mapping system

Important specifications of the ALTM are given below:

Table B.1 ALTM 1233 specifications

Laser	Nd:YAG, 1.064 micrometers
Pulse frequency	33000pps
Operating altitude:	330 to 2000 m
Range accuracy	2 cm (single-shot).
Options: Intensity data	typically 8 bit grey tones.
Number of returns recorded per laser Pulse	2
Scanner Design	Oscillating mirror
Scanner Range	± 20 degrees from nadir
Scanner Frequency	upto 30 Hz.
Data Recording	hard disk

The center has recently upgraded its capability by acquiring the latest Optech Gemini laser system capable of collecting data at a frequency of 167 kHz and registering 4 returns per laser pulse.

UF purchased a ground based laser scanning and imaging system, ILRIS 3D in 2002. It scans at a speed of 2 kHz (2000 points per second) in a range of 3m to 1500 m. It generates XYZ point clouds, together with intensity and RGB texture, provided by a built in 3.5 megapixel digital camera. ILRIS 3D operates in a static mode and therefore does not use any position or navigation sensors.

Figure B.2 ILIRIS 3D

Some of its specifications are provided below:

Table B.2 ILRIS3D specifications

Laser	Nd YAG laser, 1.55 nm, pulsed
Scanner	2 axis beam steering scanner
Data rate	2000 points per sec
Scanner Field of View	±20º horizontal as well as vertical
Range	3m to 1500m for target with 80% reflectivity; 3m to 350m for a target with 4% reflectivity
Angular accuracy	0.0024º Horizontal and Vertical
Range resolution	1 mm
Digital Camera	3.5 megapixel CMOS sensor (1789 X 1789)
Physical dimensions	320 x 320 x 220 mm, weighing 13 kg
Data storage	Removable USB memory stick, Computer hard drive through LAN network
Temperature Operating range	0ºC to 40ºC

Digital Cameras

UF houses a DuncanTech MS4100 (now distributed by Geospatial Systems Inc.) multispectral camera. It is a 3 CCD camera and can acquire images in Red, Blue, Green and Infrared band. This camera is used in combination with the ALTM system for aerial photography.

Figure B.3 MS4100 Multispectral camera

Its important specifications are mentioned below:

Table B.3 Specification for MS4100 Multispectral camera

Sensor	3 CCD with a colour separating prism
Pixel size	0.0074 mm x 0.0074 mm
Image resolution	1924 x 1075
Focal length	28 mm
Frame rate	10 frames per second
Pixel clock rate	25 MHz
Signal/Noise	60 dB
Digital image output	8 bits x 4 taps or 10 bits x 3 taps
Programmable functions	Gain, exposure time, multiplexing, trigger modes, custom processing
Electronic shutter	Range: 1/10,000 - 1/10 sec., controlled via RS-232 input
Operating Temperature	0 – 50º C

The camera can be configured to acquire RGB images or CIR images or RGB images simultaneous with monochrome IR images. It can be triggered externally through a pulse using a BNC connector and has three different operating modes for trigger input.

Recently the center bought a digital SLR camera, Nikon D80 to fully functionalize the hybrid capability of the terrestrial laser scanner, ILRIS3D.

Figure B.4 Nikon D80 digital SLR camera

The camera already integrated in the laser system gives low quality images and hence is not suited for obtaining RGB texture information of the scans. Since the application is static so a high quality point and shoot camera with the ability to be controlled externally sufficed. Some of its specifications are given below:

Table B.4 Specification for Nikon D80 SLR camera

Sensor	CCD; 23.6 x 15.88 mm
Image resolution (pixels)	Large: 3872 x 2592 (10 megapixels); Medium: 2896 x 1944 (5.6 megapixels); Small: 1936 x 1296 (2.5 megapixels)
Focal length	20 mm
Digital image output	NEF (RAW): compressed 12 bit; JPEG
ISO sensitivity	100 to 1600
External interface	USB 2.0 high speed
Physical Dimensions	132 x 103 x 77 mm; weighing 585 gms
Operating Temperature	0 – 40º C

It is controlled externally using Nikon's Camera Control Pro software. The shutter speed, aperture size and exposure compensation are a few of its important parameters which can be controlled externally.

APPENDIX C
PRINCIPAL AND NODAL POINTS

Principal Points in a Lens

Consider a ray traveling parallel to the optical axis of the lens. It undergoes refraction at the two surfaces of the thick lens. The point where the extended rays intersect is known as the rear principal point. The front principal point would be for the case when a parallel ray travels from the reverse side. The planes passing through a set of rear principal points is known as the rear principal plane. Ideally it is perpendicular to the optical axis. Similarly the plane passing through the front principal points is known as the front principal plane.

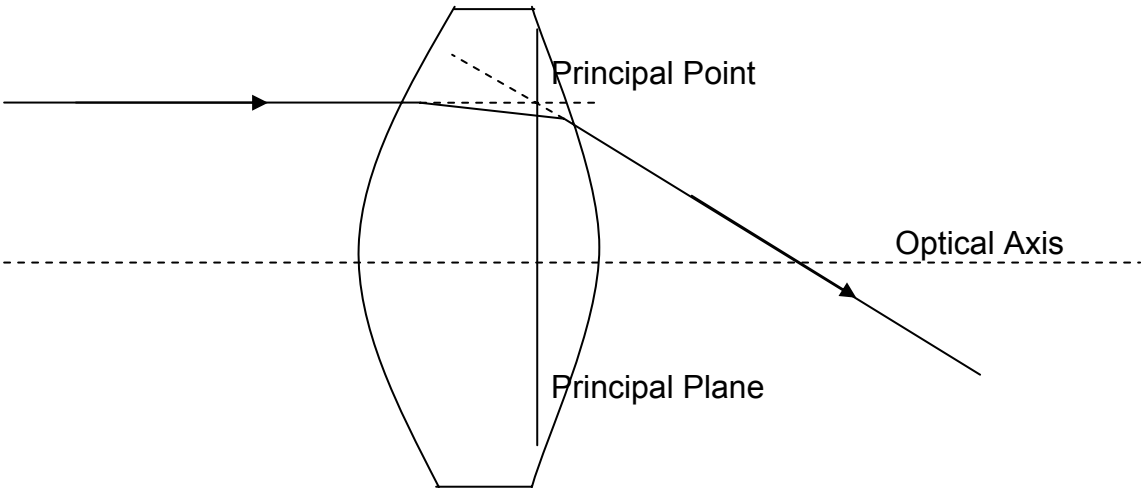

Figure C.1 Principal Points and Principal planes

Nodal Points

Consider a ray traveling at an angle to the lens striking the front face of the lens, exiting from the rear face at a different angle. Now if we start moving the ray, keeping the angle with the optical axis constant, we will find an arrival path such that the outgoing ray would exit parallel to the incoming ray. If we extend the two rays in the lens at the point of refraction, they will

intersect the optical axis at the nodal points N_1 (first nodal point) and N_2 (second nodal point). N_1 and N_2 are also called the front nodal point and the rear nodal point respectively.

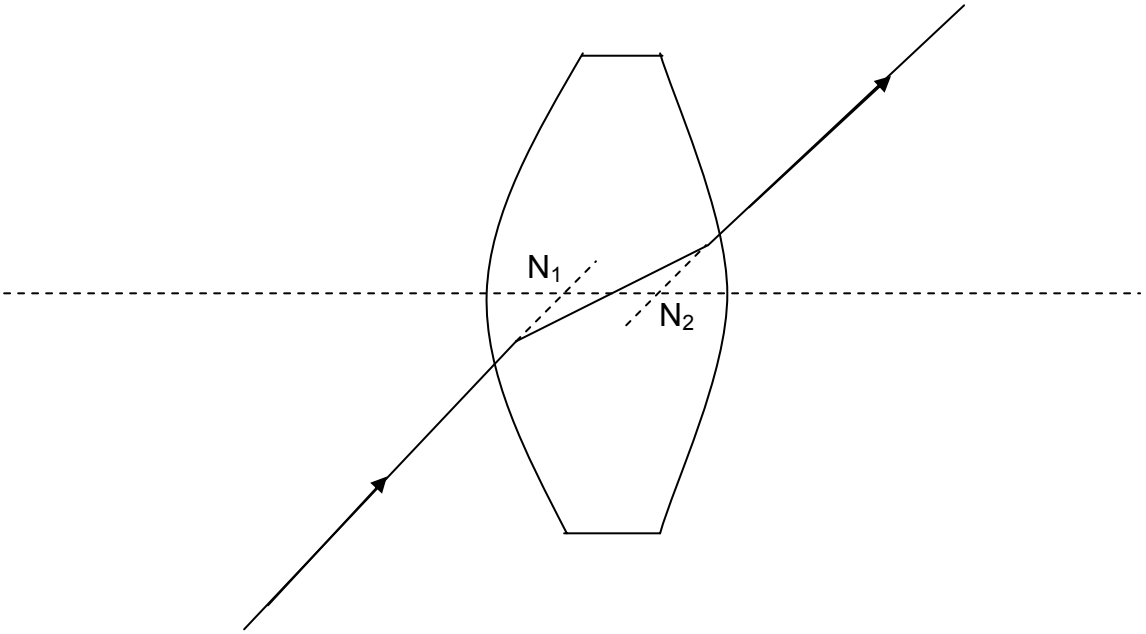

Figure C.2 Nodal Points

LIST OF REFERENCES

Abdel-Aziz Y.I. & Karara H.M., 1971. Direct linear transform from comparator coordinate into object-space coordinates. ASP/UI Symposium on Close Range Photogrammetry, Falls Church, Virginia, pp 1-18

Al Khalil, O., 2002. Solutions for exterior orientation in Photogrammetry: A review, Photogrammetric Record, 17(100), pp 615-634

Bäumker, M. & Heimes F.J., 2001. New calibration and computing method for direct georeferencing of image and scanner data using the position and angular data of an hybrid inertial navigation system, Proceedings of OEEPE-Workshop Integrated Sensor Orientation, Hannover, Germany

Cardenala, J., Mataa, E.,Castroa, P., Delgadoa, J., Hernandeza, M. A., Pereza, J.L., Ramos, M., & Torresa, M., 2004. Evaluation of a digital camera (Canon D30) for the photogrammetric recording of historical Buildings, XXth ISPRS Congress, 12 - 23 July, Istanbul, Turkey

Carter, W.E., Shrestha, R., Tuell, G., Bloomquist, & D., Sartori, M., 2001. Airborne Laser Swath Mapping shines new light on Earth's topography. American Geophysical Union EOS Transactions 82(46), pp 549, 550, 555

Chandler, J. H., Fryer, J. G. & Jack, A., 2005. Metric capabilities of low-cost digital cameras for close range surface measurement, Photogrammetric Record, 20(109). pp 12–26.

Cramer, M. & Stallman, D., 2001. On the use of GPS/inertial exterior orientation parameters in airborne photogrammetry, Proceedings of OEEPE-Workshop Integrated Sensor Orientation, Hannover, Germany

Cramer, M. & Stallman, D., 2002. System calibration for direct georeferencing. International Archives of the Photogrammetry, Remote Sensing and Spatial Information Sciences, 34(3A): 79–84

Dimitar Jechev, 2004. Close-range photogrammetry with amateur camera. Commission V, WG V/4, XXth ISPRS Congress, 12 - 23 July, Istanbul, Turkey

Drake, D.R., 2002. Applications of Laser Scanning and Imaging Systems, Unpublished Master's Thesis, University of Florida

Fernandez, J.C., 2007. Scientific Applications of Mobile Terrestrial Laser Scanner (M-TLS) System, Unpublished Master's Thesis, University of Florida

Fraser, C.S., 1982. On the use of non-metric cameras in analytical non-metric photogrammetry, International Archives of Photogrammetry and Remote Sensing, 24(5), pp. 156-166

Fraser, C.S., 1997. Digital camera self-calibration, ISPRS Journal of Photogrammetry and Remote Sensing, 52, pp. 149-159

Fraser, C.S., 2001. Photogrammetric camera component calibration: A review of analytical techniques in Calibration and Orientation of Cameras in Computer Vision, Gruen & Huang (Eds.), Springer Series in Information Sciences 34, New York, pp 95-121

Grennery, D.B., 2001. Least squares camera calibration including Lens Distortion and automatic editing of calibration points in Calibration and Orientation of Cameras in Computer Vision, Gruen & Huang (Eds.), Springer Series in Information Sciences 34, New York, pp 163-193

Grejner-Brzezinska D.A., Direct sensor orientation in airborne and land-based mapping applications, http://www.ceegs.ohio-state.edu/gsreports/reports/report_461.pdf, last accessed: August 6, 2007

Gruen, A.& Beyer, H.A., 2001. System calibration through self-calibration in Calibration and Orientation of Cameras in Computer Vision, Gruen & Huang (Eds.), Springer Series in Information Sciences 34, New York, pp 163-193

Heikkilä J. & Silven O., 1997. A four-step camera calibration procedure with implicit image correction. Proceedings of IEEE Conference on Computer Vision and Pattern Recognition, San Juan, Puerto Rico, pp 1106-1112

History of Photogrammetry, 2007. The Center for Photogrammetric Training Surveying Engineering Department, Ferris State University, Big Rapids, Michigan http://www.ferris.edu/faculty/burtchr/sure340/notes/History.pdf, last accessed: August 7, 2007

Jansa, J., Studnicka, N., Forkert, G., Haring, A., & Kager, H., 2004. Terrestrial laser scanning and photogrammetry – Acquisition techniques complementing one another, Commission III WG 7**,** XXth ISPRS Congress, Istanbul, Turkey

Jacobsen, K., 2000. Potential and Limitation of Direct Sensor Orientation. International Archives of Photogrammetry and Remote Sensing, 33(B3/1), pp 429–435

Jacobsen, K., 2002. Calibration Aspects in Direct Georeferencing Of Frame Imagery. International Archives of the Photogrammetry, Remote Sensing and Spatial Information Sciences, 34(1), pp 82–89

Kolbel, O R., 1976. Metric or nonmetric camera, Photogrammetric Enginnering and Remote Sensing, 42(1), pp 103-113

Linder, W., 2006. Digital Photogrammetry: A Practical Course, Second Edition, Springer ,

Mohr, R. & Bill Triggs, B., 1996. Projective geometry for image analysis: Tutorial on projective geometry. XVIII ISPRS Congress Vienna, Austria

Nagai, M., Shibasaki, R., Manandhar, D. & Zhao, H., 2004. Development of digital surface model and feature extraction by integrating laser scanner and CCD sensor with IMU. XXth ISPRS Congress, Istanbul, Turkey

Naci, Y. & Karsten, J., 2005. Influence of system calibration on direct sensor orientation, Photogrammetric Engineering and Remote Sensing, 71(5), pp. 629

Pinto, L. & Forlani, G., 2002. A single step calibration procedure for IMU/GPS in aerial photogrammetry, Proceedings of the ISPRS Technical Commission III Symposium, Graz, Austria

Remondino, F. & Borlin, N., 2004. Photogrammetric calibration of image sequences acquired with a rotating camera, Proceedings of the ISPRS working group V/1, Panoramic Photogrammetry Workshop, Dresden, Germany

Remondino, F. & Fraser, C.S., 2006. Digital camera calibration methods: considerations and comparisons. International Archives of Photogrammetry, Remote Sensing and Spatial Information Sciences, Vol. XXXVI, part 5, pp. 266-272 ISPRS Commission V Symposium, Dresden, Germany

Rogers, R.M.; 2003. Applied mathematics in integrated navigation systems, Second edition

Ruzgienė, B., 2005. Performance Evaluation of Non-Metric Digital Camera for Photogrammetric Application, Geodesy and Cartography, 31(1), pp 23-27

Tsai, R., 1987, A versatile camera calibration technique for high accuracy 3-D machine vision metrology using off-shelf TV cameras and lenses. IEEE Journal of Robotics and Automation, 3(4), pp 323-344

Ullrich, A., Schwarz, R. & Kager, H. 2003. Using hybrid multi-station adjustment for an integrated camera laser-scanner system. Optical 3-D Measurement Techniques, 6(1), pp 298-305

US Army Corps of Engineers. 2003. NAVSTAR Global Positioning System Surveying, Engineer Manual

Wackrow , R., Chandler, J.H. & Bryan, P., 2007. Geometric consistency and stability of consumer-grade digital cameras for accurate spatial measurement, The Photogrammetric Record, 22(118), pp 121-134

Wolf, P. & Dewitt, B., 2002. Elements of Photogrammetry with Applications in GIS, Third edition

Yakimovsky, Y., 1987.Cunningham, R.T., A system for extracting three-dimensional measurements from a stereo pair of TV cameras, Computer Graphics and Image Processing, 7, pp 195-210

BIOGRAPHICAL SKETCH

Abhinav Singhania was born in Patna, India, on December 27, 1982. He graduated with a Bachelor of Engineering degree in civil engineering from Punjab Engineering College, Chandigarh, India, in May 2005. His interests in remote sensing led him to University of Florida where he worked with the Geosensing Systems Engineering group and graduated with a Master of Science degree in civil engineering in December 2007.